

Abstract

The socioeconomic losses from the recent unpreceded incidents in the electric power systems suggest the need for alternative planning strategies that account for the expected and extreme events that are less likely to occur. Such high impact low probability (HILP), or black swan, events are typically weather-related, have accounted for billions of dollars in economic losses, and left customers in the dark for several days. Furthermore, the proliferation of distributed energy resources (DERs) on the distribution grid indicates that system operators can also plan resilience from the customer's end, forming intentional microgrid islands when needed. However, existing planning strategies only minimize the expected operating cost and do not explicitly include the risk of extreme events. With the increasing frequency of black swan events in the current scenario, system operators should focus on the HILP events and find the optimal trade-off decision to maximize resilience with available resources. This proposal aims to investigate the impact of extreme weather events, hurricanes, and floods, on the power grid and propose planning solutions to enhance the grid's resilience. Firstly, we propose a modeling framework to assess the spatiotemporal compounding effect of hurricanes and storm surges on electric power systems. The spatiotemporal probabilistic loss metric helps system operators identify the potential impact and vulnerable components as the storm approaches. Secondly, we develop a risk-averse two-stage stochastic optimization framework for resilience planning of power distribution systems against extreme weather events. The resource planning strategy involves minimizing a risk metric, conditional value-at-risk (CVaR) while adhering to budget constraints for planning. The main idea is to identify a trade-off between risk-averse and risk-neutral planning solutions to maximize the energization of critical loads when a HILP event is realized. The problem is also extended to determine the trade-off among different resources when system operators have a limited budget. This facilitates the selection of specific resources from a portfolio of various resources that can optimally restore critical loads during the realization of a HILP event. In the future, the work will be extended to a larger and broader landscape with an analysis based on realistic extreme weather events and their impact on the power system. The goal will be to create a generic simulation platform capable of generating and assessing the impact of such events on the electric power grid. The work will also include large-scale integrated operational solutions to enhance the resilience of future power grids. Furthermore, advanced parallel algorithms based on dual decomposition methods will be explored for scalable implementation of stochastic programming problems.

Contents

1 Motivation	5
2 Objectives and Task Lists	7
3 MPOPF Modelling Tradeoffs: Linear vs Nonlinear Formulations	9
3.1 Introduction	9
3.2 MPOPF Problem Definition	9
3.3 Formulation Comparison	10
3.4 Performance Metrics	10
3.5 Empirical Evaluation	10
3.5.1 Test Systems	10
3.5.2 Workflow	11
3.5.3 Results	11
3.6 Discussion	12
3.7 Conclusions	13
4 Spatial Decomposition via Equivalent Network Approximation (ENApp)	15
4.1 Introduction and Motivation	15
4.2 Problem Formulation	17
4.2.1 Notations	17
4.2.2 MPCOPF with Batteries	18
4.2.3 ENApp-based MPDOPF with Batteries	19
4.3 Case Study Demonstration: IEEE 123 Bus Test System	20
4.3.1 Test System Description	20
4.3.2 Simulation Workflow	20
4.4 Simulation Results and Performance Analysis	21
4.4.1 5-Hour Horizon Results	21
4.4.2 10-Hour Horizon: Scalability Analysis	24
4.5 Summary and Discussion	26
4.5.1 Key Observations	28
4.5.2 Implementation Status and Future Work	29
5 Temporal Decomposition via Differential Dynamic Programming	31
5.1 Introduction	31
5.2 DDP Algorithm for MPOPF	31
5.3 Computational Advantages for Long-Horizon MPOPF	33
5.4 Relationship to Other Decomposition Methods	34
5.5 Numerical Results: 24-Hour Horizon on IEEE 123-Bus System	34

5.5.1	System Configuration and Convergence	34
5.5.2	Performance Summary	36
5.5.3	Preliminary Results on Larger Systems	37
5.6	Summary	38
6	Temporal Decomposition via Temporal Alternating Direction Method of Multipliers (tADMM)	42
6.1	Introduction and Motivation	42
6.2	LinDistFlow MPOPF with tADMM	43
6.2.1	Problem Overview	43
6.2.2	Variable Color Coding	43
6.2.3	Sets and Indices	43
6.2.4	tADMM Algorithm Structure	44
6.2.5	Convergence Criteria	46
6.3	Copper Plate MPOPF with tADMM (Simplified Case)	47
6.3.1	Problem Overview	47
6.3.2	Variable Color Coding	47
6.3.3	tADMM Algorithm Structure	47
6.4	Numerical Results	50
6.4.1	Battery Actions and Convergence Analysis	50
6.5	Convergence Criteria	51
6.5.1	Convergence Criteria	51
6.6	Algorithm Parameters	52
6.6.1	Objective Function Components	52
6.6.2	Algorithmic Parameters	53
6.7	Appendix: Full Variable and Parameter Definitions	53
6.7.1	System Bases	53
6.7.2	SOC Bound Definitions	53
6.7.3	Physical Interpretation	53
6.8	Summary and Discussion	54
6.8.1	Implementation Status	54
7	Future Works	57
7.1	Task 1: Temporal Decomposition for Medium Sized Balanced Three-Phase Systems	57
7.2	Task 2: Temporal Decomposition for Large Sized Unbalanced Three-Phase Systems	57
7.3	Task 3: Concluding Research and Dissertation	58
7.4	Timeline	59

8	Biography	60
8.1	Publications	60
8.2	Program of Study Course Work	61
Appendix		62
.1	Full MPOPF Formulation with LinDistFlow	62

1 Motivation

Optimal power flow (OPF) methods have become vital for efficiently managing distributed energy resources (DERs) such as photovoltaic (PV) and battery energy storage systems (BESS) at the grid edge, aiming to enhance system-level objectives including reliability, resilience, and cost-effectiveness [1, 2]. BESS, by mitigating the fluctuations of intermittent DERs, transforms the OPF problem from a classic single-period formulation into a multi-period, time-coupled optimization that demands intricate modeling and advanced computational methods [1, 3].

Centralized OPF (COPF) approaches typically rely on non-convex formulations—often based on the nonlinear branch flow model [4]—to coordinate controllable devices. Although such methods can provide accurate solutions for small networks [1, 3, 5], computational time and scalability issues limit their utility in large-scale, real-world systems. Metaheuristic and evolutionary algorithms [6] offer alternative solutions but generally struggle with local optimality and slow convergence, especially for high-dimensional multi-period OPF tasks.

To improve tractability, convex relaxations and linear approximations such as LinDistFlow [7] have been widely employed [1, 3, 7]. These methods deliver fast convergence but introduce non-negligible optimality gaps, particularly as network size and DER/BESS penetration increase, which has not been fully quantified in existing research [1]. Recent studies have highlighted this gap, advocating for a systematic comparison of non-convex and linearized frameworks across varied network conditions [1, 7].

Recognizing the limitations of centralized and linear-programming-based solutions, recent research—including our own—has focused on spatial and temporal decomposition for scalable multi-period OPF. Our group adapted the Equivalent Network Approximation (ENApp) framework to enable distributed MPOPF (MPDOPF) in battery-integrated networks, leveraging spatial partitioning to allow parallel solution of local OPF subproblems and reduce global computational burdens [8]. This approach harnesses the radial structure of distribution networks and significantly accelerates convergence while maintaining solution fidelity. Moreover, our models introduce a battery loss term exclusively in the objective function, preventing simultaneous charge/discharge operations and preserving problem convexity without integer variables [8].

Extensive validation against industry-standard IEEE test systems demonstrates that our ENApp-based distributed MPOPF delivers superior scalability and optimality compared with conventional centralized frameworks. These studies also provide a robust, side-by-side comparison of LinDistFlow and branch flow-based nonlinear models for MPOPF across real

distribution network scenarios [1].

Major remaining research gaps include the scalability and real-time applicability of centralized MPOPF approaches [3, 5, 9–11], and the slow convergence and master controller dependencies in existing distributed frameworks such as Benders decomposition [12]. The contribution of this work is the development and benchmarking of a spatially distributed multi-period OPF algorithm, overcoming these challenges and enabling practical, accurate, large-scale coordinated grid-edge resource management.

2 Objectives and Task Lists

The overarching goal of this work is to develop a computationally scalable framework for solving the Multi-Period Optimal Power Flow (MPOPF) problem in active distribution systems. The proposed framework aims to address the inherent complexity and non-convexity of MPOPF formulations – arising from temporal coupling of decision variables and high-dimensional system models – by designing and implementing decomposition-based algorithms. The resulting framework is expected to enable tractable and near-optimal solutions for realistic time horizons and large distribution feeders, while preserving the physical fidelity of the underlying models. The following tasks have been completed or are currently being pursued toward achieving the objectives of this study:

1. **Literature Review on Multi-Period Optimal Power Flow:** A comprehensive review was conducted on existing formulations of the MPOPF problem for active distribution systems. This provided insights into modeling temporal dependencies, handling storage dynamics, and integrating distributed energy resources in multi-period settings.
2. **Study of Decomposition-Based Optimization Techniques:** A review of decomposition algorithms, including Bilevel optimization methods, ADMM, and Differential Dynamic Programming (DDP), was carried out to understand their suitability for large-scale and temporally coupled optimization problems. The study highlighted key convergence properties and trade-offs between spatial and temporal decompositions.
3. **Implementation of Spatial Decomposition for MPOPF:** A spatially decomposed MPOPF formulation was implemented and tested on benchmark distribution systems. The method demonstrated improved scalability compared to monolithic optimization, though it remained limited in addressing the temporal coupling present in long-horizon studies.
4. **Development and Evaluation of Differential Dynamic Programming (DDP):** The DDP algorithm was formulated and implemented for the MPOPF problem. While the approach yielded solutions close to those obtained from brute-force optimization, it exhibited oscillatory convergence behavior and lacked strong theoretical guarantees. Further research is required to enhance its stability and convergence properties.
5. **Implementation of Temporal ADMM for MPOPF:** A temporal Alternating Direction Method of Multipliers (ADMM) approach is being developed to address the

scalability challenges associated with increasing time horizons. Preliminary results on a copper-plate system show excellent convergence, and current efforts focus on extending the implementation to LinDistFlow-based distribution models.

6. **Validation and Scalability Testing:** The final phase will involve validating the proposed algorithms on a large-scale system like the 9500-node (three-phase) feeder. The goal is to demonstrate the framework's scalability for realistic horizons (e.g., $T = 96$ i.e. 1 day at 15-minute intervals) and its applicability to operational optimization in distribution grids.
7. **Exploratory Study on Multiple-Source Optimal Power Flow (MS-OPF):** As a future research direction, the framework will be extended to accommodate multi-source configurations, enabling coordinated optimization across multiple substations and zones in distribution networks.

3 MPOPF Modelling Tradeoffs: Linear vs Nonlinear Formulations

3.1 Introduction

Before applying spatial or temporal decomposition to multi-period optimal power flow (MPOPF) problems, a critical decision must be made: **which power flow formulation to use?** This chapter compares two approaches:

1. **Nonlinear Branch Flow Model (BFM-NL)** [13]: Accurate non-convex programming, computationally expensive
2. **LinDistFlow** [7]: Fast linear programming with approximation errors

Key Insight: The formulation choice shapes any decomposition algorithm built upon it. Even if decomposition converges correctly, a flawed base formulation propagates errors.

This chapter establishes theoretical foundations (problem definition, formulations, performance metrics), then presents empirical results demonstrating the tradeoffs for systems of varying scales and grid-edge device (GED) penetrations.

3.2 MPOPF Problem Definition

3.2.0.1 System Model: Radial distribution network as a tree with buses \mathcal{N} , lines \mathcal{L} , time horizon $\tau = \{1, \dots, T\}$, load buses $\mathcal{N}_{\mathcal{L}}$, PV buses $\mathcal{D} \subseteq \mathcal{N}_{\mathcal{L}}$, battery buses $\mathcal{B} \subseteq \mathcal{N}_{\mathcal{L}}$.

3.2.0.2 Key Variables: $v_j^t = (V_j^t)^2$ (squared voltage), $l_{ij}^t = (I_{ij}^t)^2$ (squared current), P_{ij}^t, Q_{ij}^t (line flows), $p_{D_j}^t, q_{D_j}^t$ (PV output), $P_{c_j}^t, P_{d_j}^t, q_{B_j}^t$ (battery power), B_j^t (battery energy), P_{Subs}^t (substation power), C^t (electricity cost).

3.2.0.3 Objective Function: Minimize total substation cost plus penalty for simultaneous charge-discharge [14]:

$$\min \sum_{t=1}^T \left\{ C^t P_{Subs}^t \Delta t + \alpha \sum_{j \in \mathcal{B}} \left[(1 - \eta_c) P_{c_j}^t + \left(\frac{1}{\eta_d} - 1 \right) P_{d_j}^t \right] \right\} \quad (1)$$

3.3 Formulation Comparison

Table 1 contrasts the two formulations.

Table 1: BFM-NL vs LinDistFlow formulation comparison

Constraint	BFM-NL	LinDistFlow
Real power balance	$\sum_k P_{jk}^t - (P_{ij}^t - r_{ij}l_{ij}^t) = p_j^t$	$\sum_k P_{jk}^t - P_{ij}^t = p_j^t$
Reactive power balance	$\sum_k Q_{jk}^t - (Q_{ij}^t - x_{ij}l_{ij}^t) = q_j^t$	$\sum_k Q_{jk}^t - Q_{ij}^t = q_j^t$
Voltage drop (KVL)	$v_j^t = v_i^t - 2(r_{ij}P_{ij}^t + x_{ij}Q_{ij}^t) + (r_{ij}^2 + x_{ij}^2)l_{ij}^t$	$v_j^t = v_i^t - 2(r_{ij}P_{ij}^t + x_{ij}Q_{ij}^t)$
Power-current relation	$(P_{ij}^t)^2 + (Q_{ij}^t)^2 = l_{ij}^t v_i^t$	Not modeled
Battery inverter	$(P_{B_j}^t)^2 + (q_{B_j}^t)^2 \leq S_{B_{R,j}}^2$	Hexagonal approx. [15]

Key Differences: BFM-NL includes loss terms $(r_{ij}l_{ij}^t, x_{ij}l_{ij}^t)$ and quadratic constraints; LinDistFlow drops these for linearity, introducing approximation errors.

Common Constraints: Voltage limits $v_j^t \in [V_{min}^2, V_{max}^2]$, battery dynamics $B_j^t = B_j^{t-1} + \Delta t(\eta_c P_{c_j}^t - \eta_d^{-1} P_{d_j}^t)$, power limits, SOC bounds.

3.4 Performance Metrics

3.4.0.1 Optimality: Gap between objective values:

$$\text{Optimality Gap (\%)} = \frac{\text{Cost}_{\text{LinDistFlow}} - \text{Cost}_{\text{BFM-NL}}}{\text{Cost}_{\text{BFM-NL}}} \times 100 \quad (2)$$

3.4.0.2 Feasibility: Discrepancies when control set-points are validated in OpenDSS (AC power flow):

$$\Delta V = \max_{j,t} |V_{j,\text{OpenDSS}}^t - V_{j,\text{model}}^t|, \quad \Delta P_{Subs} = \max_t |P_{Subs,\text{OpenDSS}}^t - P_{Subs,\text{model}}^t| \quad (3)$$

3.4.0.3 Computational Efficiency: Wall-clock solve time (seconds) using Ipopt [16] via JuMP [17].

3.5 Empirical Evaluation

3.5.1 Test Systems

Three systems with increasing size and GED penetration (PV%/BESS%):

- **ADS10**: 10-bus, 25%/25%, 33% sizing (Figure 1)
- **IEEE123A**: 128-bus, 20%/30%, 33% sizing (Figure 2)
- **IEEE123B**: 128-bus, 30%/50%, 100% sizing

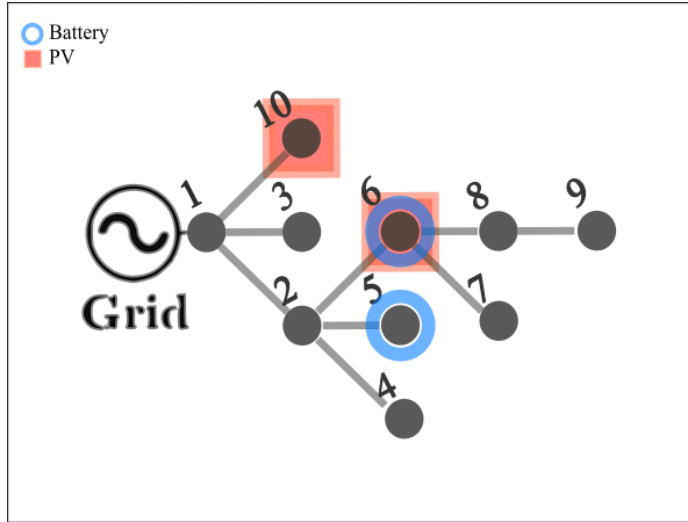


Figure 1: ADS10: 10-bus system

All systems use 24-hour forecasts (Figure 3) with bilevel pricing. Parameters: $T = 24$ h, $\Delta t = 1$ h, $V_{min/max} = 0.95/1.05$ pu, $\eta_c = \eta_d = 0.95$, $soc_{min/max} = 0.30/0.95$, 4-hour battery storage.

3.5.2 Workflow

Models built in JuMP, solved with Ipopt (cold start). Control set-points validated in OpenDSS via OpenDSSDirect.jl [18]. Code: [19].

Note: LinDistFlow[®] denotes LinDistFlow controls evaluated in OpenDSS (to account for actual losses).

3.5.3 Results

Table 2 summarizes key findings across all three systems.

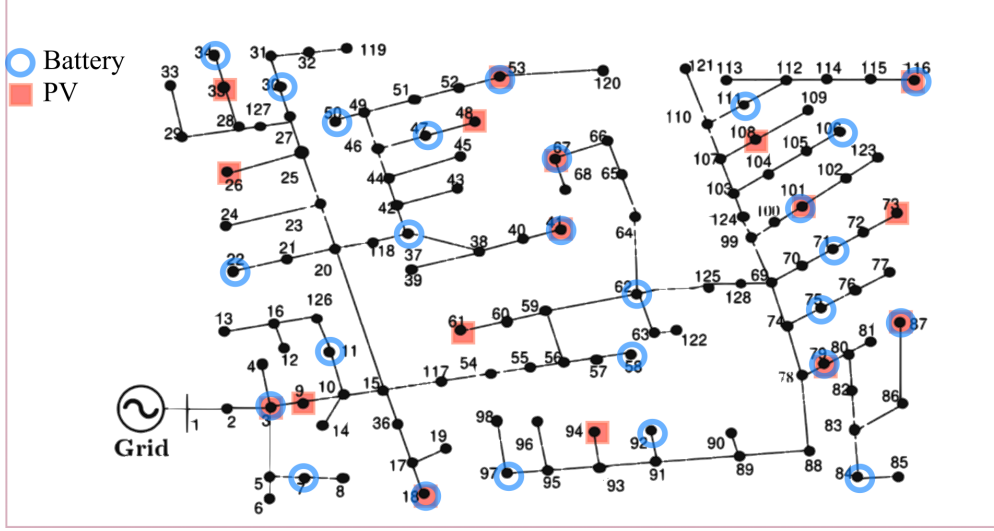


Figure 2: IEEE-123: 128-bus system

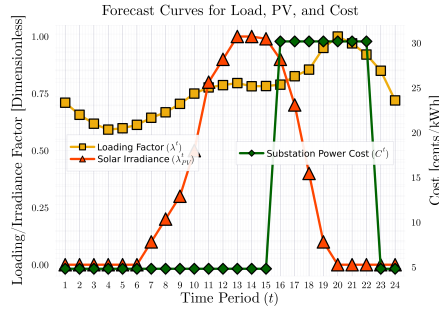


Figure 3: 24-hour forecasts: load, irradiance, cost

3.6 Discussion

3.6.0.1 Optimality Gap: Grows from 0.005% (ADS10) to 0.71% (IEEE123B) due to: (1) larger line losses not captured by LinDistFlow, (2) higher battery penetration amplifying hexagonal approximation error. **Implication:** For decomposition algorithms, LinDistFlow provides acceptable cost approximations for small-moderate systems but degrades with scale.

3.6.0.2 Computational Speedup: LinDistFlow achieves $3\times$ – $20\times$ faster solve times by eliminating nonlinear constraints. **Implication:** Useful for rapid initialization or warm-starting BFM-NL-based decomposition.

Table 2: Performance summary: BFM-NL vs LinDistFlow

Metric	ADS10		IEEE123A		IEEE123B	
	BFM-NL	LinDF [©]	BFM-NL	LinDF [©]	BFM-NL	LinDF [©]
Cost (\$)	204.27	204.28	2787.44	2798.4	1973.83	1987.78
Optimality gap (%)	0.005		0.39		0.71	
Solve time (s)	2.64	0.77	17.44	0.85	23.75	1.66
Speedup	$3.4\times$		$20.5\times$		$14.3\times$	
ΔV (pu)	0.00001	0.00001	0.00007	0.00206	0.00006	0.00160
ΔP_{Subs} (kW)	0.00001	0.02	0.43	32.36	0.22	23.34

3.6.0.3 Reactive Power Mismanagement: LinDistFlow allocates $10\times\text{--}18\times$ less reactive power to distributed inverters compared to BFM-NL (e.g., IEEE123A: 195 vs 1972 kVARh for PVs), concentrating support at the substation. This stems from omitting the $l_{ij}^t x_{ij}$ term that couples reactive flow to losses. **Implication:** Under-utilizes grid support capability; risky for voltage regulation objectives.

3.6.0.4 Substation Power Underprediction: LinDistFlow underestimates hourly substation power by up to 32 kW (2–5%), creating risks: equipment overloads, reserve margin violations, economic errors. **Implication:** Decomposition algorithms using LinDistFlow will systematically underpredict system-level quantities.

3.6.0.5 Recommended Strategy: Hybrid approach for decomposition: (1) Initialize with LinDistFlow for speed, (2) Refine with BFM-NL for accuracy, (3) Validate with OpenDSS before deployment. This balances computational tractability with solution quality.

3.7 Conclusions

The formulation choice (BFM-NL vs LinDistFlow) fundamentally determines the behavior of any spatial or temporal decomposition algorithm. Key takeaways:

- **Optimality:** LinDistFlow introduces 0.4–0.7% gap for moderate-large systems
- **Reactive Power:** LinDistFlow systematically misallocates reactive resources
- **Feasibility:** Substation power errors up to 5% create operational risks

- **Speed:** $10\text{--}20\times$ computational advantage enables rapid scenario analysis

For the spatial (ENApp) and temporal (ADMM) decomposition algorithms in subsequent chapters, this analysis informs whether to use BFM-NL (accurate but slow), LinDistFlow (fast but approximate), or a hybrid strategy depending on system scale and accuracy requirements.

The aim of this thesis is to develop decomposition algorithms based on the accurate BFM-NL formulation to ensure high-fidelity solutions for large-scale MPOPF problems.

But it is also important to recognize the potential role of LinDistFlow in initialization or warm-starting to accelerate convergence without sacrificing final solution quality.

4 Spatial Decomposition via Equivalent Network Approximation (ENApp)

4.1 Introduction and Motivation

Optimal power flow (OPF) methods are employed to optimally coordinate grid’s controllable resources for different system-level objectives, such as economic operations, reliability, and resilience. The significance of OPF studies is growing in relevance at the distribution system level, driven by the increasing adoption of distributed energy resources (DERs), particularly photovoltaic systems (PVs) and battery energy storage systems (BESS). Furthermore, the adoption of BESS is gaining significance for managing the variability of DERs through controlled charging and discharging, thereby ensuring supply-demand balance [20]. Incorporating BESS into OPF problems substantially raises the complexity of network optimization problems, transitioning from a single-period, time-decoupled OPF to a multi-period, time-coupled OPF.

Traditionally, centralized OPF (COPF) methods have been widely used, where a central controller processes aggregated grid-edge data, executes the OPF algorithm, and sends control signals to manage resources [21]. The COPF algorithms for DER management are generally developed as a mixed integer non-convex programming (MINCP) problem and then simplified either as a convex problem by adopting second-order cone programming (SOCP) relaxations [22] [23], or as a linear problem by adopting Taylor series expansion [21], polyhedral approximations [24] or linear power flow models [25]. Unfortunately, COPF methods pose scalability challenges for larger networks and for difficult classes of OPF problems such multi-period time-coupled formulations required to optimally manage BESS.

To address scalability challenges, distributed OPF (DOPF) algorithms have been introduced. These algorithms decompose the COPF problem into smaller sub-problems that are solved concurrently, leveraging communication among neighboring areas. In this context, the Auxiliary Problem Principle (APP) and the Alternating Direction Method of Multipliers (ADMM) are widely adopted algorithms for solving various OPF problems, including non-convex formulations [26], convex-relaxed versions [27–29], and linear approximations [30]. Similarly, in a prior study [31], the authors’ research group introduced a DOPF framework utilizing the Equivalent Network Approximation method (ENApp). This approach was shown to require fewer macro iterations compared to traditional ADMM or APP algorithms for solving DOPF problems.

The above references [22]- [30] mainly focused on solving single time-period OPF prob-

lems and did not include the coordination of grid-edge devices that introduce time-coupled constraints, such as BESS. The inclusion of BESS models results in a multi-period OPF (MPOPF) problem with time-coupled constraints. Reference [5] proposed a nonlinear multi-period centralized OPF (MPCOPF) approach to optimally coordinate active-reactive power dispatch from batteries and DERs in distribution systems. Alizadeh and Capitanescu [32] proposed a stochastic security-constrained MPCOPF, which sequentially solves a specific number of linear approximations of the original problem. Usman and Capitanescu [33] developed three different MPCOPF frameworks. All three approaches begin by solving a linear program to optimize the binary variables first, followed by either a linear or non-linear program to optimize the continuous variables. Optimal battery schedules are determined in [34] considering uncertain renewable power generation by solving an MPCOPF. A bi-level robust MPCOPF is suggested in [35] for determining active and reactive power dispatches from the grid edge devices. Wu et al. [12] framed a Benders Decomposition (BD) based multi-period distributed OPF (MPDOPF) after decomposing the original centralized multi-parametric quadratic problem into one master and multiple sub-problems.

Over recent years, numerous research efforts have focused on developing MPOPF methodologies. However, the following research gaps persist:

1. The MPOPF models are mainly solved centrally [5]- [35]. The centralized methods suffer from scalability and computational challenges, requiring significantly long solution times, rendering them unsuitable for operational decision-making.
2. Reference [12] proposed a MPDOPF framework using Benders Decomposition. However, this approach suffers from slow convergence and needs a central controller to solve the master problem.

This work aims to address the above research gaps by developing a spatially distributed MPOPF (MPDOPF) framework. The distribution system is divided into multiple connected areas, each solving its own local MPOPF problem and periodically communicating the values of boundary variables with neighboring areas. The interaction between the areas is modeled by following the principles of the ENApp DOPF algorithm. ENApp outperforms the other DOPF algorithms in terms of convergence speed and requires fewer macro iterations [31]. The specific contributions of this work are listed below:

1. A MPOPF framework is proposed for distribution systems consisting of DERs and batteries. The integer variables related to battery charging/discharging are avoided by

adding a “Battery Loss” cost term in the objective function. The loss term will ensure the non-occurrence of simultaneous charging/discharging operations.

2. The original MPOPF framework is solved in a distributed manner by following the principles of the ENApp-based distributed OPF. This provides faster convergence and requires less solution time compared to the traditional MPCOPF.
3. Detailed comparative analyses between traditional MPCOPF and the proposed MP-DOPF are done using the IEEE 123 bus test system and the benefits of the proposed approach are demonstrated. ACOPF feasibility validation is also performed by implementing the derived controls into an OpenDSS model of the test system.

4.2 Problem Formulation

4.2.1 Notations

In this study, the distribution system is modeled as a tree (connected graph) with N number of buses (indexed with i , j , and k); the study is conducted for T time steps (indexed by t), each of interval length Δt . The sets of buses with DERs and batteries are D and B respectively, such that $D, B \subseteq N$. A directed edge from bus i to j in the tree is represented by ij and the set for edges is given by \mathcal{L} . Line resistance and reactance are r_{ij} and x_{ij} , respectively. Magnitude of the current flowing through the line at time t is denoted by I_{ij}^t and $l_{ij}^t = (I_{ij}^t)^2$. The voltage magnitude of bus j at time t is given by V_j^t and $v_j^t = (V_j^t)^2$. Apparent power demand at a node j at time t is $s_{L_j}^t$ ($= p_{L_j}^t + j q_{L_j}^t$). The active power generation from the DER present at bus j at time t is denoted by $p_{D_j}^t$ and controlled reactive power dispatch from the DER inverter is $q_{D_j}^t$. DER inverter capacity is $S_{D_{R_j}}$. The apparent power flow through line ij at time t is S_{ij}^t ($= P_{ij}^t + j Q_{ij}^t$). The real power flowing from the substation into the network is denoted by P_{Subs}^t and the associated cost involved per kWh is C^t . The battery energy level is B_j^t . Charging and discharging active power from battery inverter (of apparent power capacity $S_{B_{R_j}}$) are denoted by $P_{c_j}^t$ and $P_{d_j}^t$, respectively and their associated efficiencies are η_c and η_d , respectively. The energy capacity of the batteries is denoted by B_{R_j} , and the rated battery power is $P_{B_{R_j}}$. soc_{min} and soc_{max} are fractional values for denoting safe soc limits of a battery about its rated state-of-charge (soc) capacity. The reactive power support of the battery inverter is indicated by $q_{B_j}^t$.

4.2.2 MPCOPF with Batteries

The OPF problem aims to minimize two objectives as shown in eq. (4). The first term in eq. (4) aims to minimize the total energy cost for the entire horizon. Including the ‘Battery Loss’ cost as the second term ($\alpha > 0$) helps eliminate the need for binary (integer) variables typically used to prevent simultaneous charging and discharging. The resulting OPF problem is a non-convex optimization problem [14].

$$\min \sum_{t=1}^T \left[C^t P_{Subs}^t \Delta t + \alpha \sum_{j \in \mathcal{B}} \left\{ (1 - \eta_C) P_{C_j}^t + \left(\frac{1}{\eta_D} - 1 \right) P_{D_j}^t \right\} \right] \quad (4)$$

Subject to the constraints eqs. (5) to (15) as given below:

$$\begin{aligned} \sum_{(j,k) \in \mathcal{L}} \{P_{jk}^t\} - (P_{ij}^t - r_{ij} l_{ij}^t) &= (P_{d_j}^t - P_{c_j}^t) \\ &+ p_{D_j}^t - p_{L_j}^t \end{aligned} \quad (5)$$

$$\sum_{(j,k) \in \mathcal{L}} \{Q_{jk}^t\} - (Q_{ij}^t - x_{ij} l_{ij}^t) = q_{D_j}^t + q_{B_j}^t - q_{L_j}^t \quad (6)$$

$$v_j^t = v_i^t - 2(r_{ij} P_{ij}^t + x_{ij} Q_{ij}^t) + \{r_{ij}^2 + x_{ij}^2\} l_{ij}^t \quad (7)$$

$$(P_{ij}^t)^2 + (Q_{ij}^t)^2 = l_{ij}^t v_i^t \quad (8)$$

$$P_{Subs}^t \geq 0 \quad (9)$$

$$v_j^t \in [V_{min}^2, V_{max}^2] \quad (10)$$

$$q_{D_j}^t \in \left[-\sqrt{{S_{D_{R,j}}}^2 - {p_{D_j}^t}^2}, \sqrt{{S_{D_{R,j}}}^2 - {p_{D_j}^t}^2} \right] \quad (11)$$

$$B_j^t = B_j^{t-1} + \Delta t \eta_c P_{c_j}^t - \Delta t \frac{1}{\eta_d} P_{d_j}^t \quad (12)$$

$$P_{c_j}^t, P_{d_j}^t \in [0, P_{B_{R_j}}], \quad B_j^0 = B_j^T \quad (13)$$

$$q_{B_j}^t \in [-\sqrt{0.44} P_{B_{R,j}}, \sqrt{0.44} P_{B_{R,j}}] \quad (14)$$

$$B_j^t \in [soc_{min} B_{R,j}, soc_{max} B_{R,j}] \quad (15)$$

A branch power flow model, given by eqs. (5) to (8), is used to represent power flow in distribution system. Constraints eqs. (5) and (6) model the active and reactive power balance at node j , respectively. The KVL equation for branch (ij) is represented by eq. (7), while the equation describing the relationship between current magnitude, voltage magnitude and apparent power magnitude for branch (ij) is given by eq. (8). Backflow of real power into the substation from the distribution system is avoided using the constraint eq. (9). The allowable limits for bus voltages are modeled via eq. (10). eq. (11) describes the reactive power limits of DER inverters. The trajectory of the battery energy versus time is given by eq. (12) (this is a time-coupled constraint). Battery charging and discharging powers are limited by the battery's rated power capacity, as given by eq. (13). eq. (13) also says that the initial and final energy levels for battery must be the same at the end of the optimization time horizon. Every battery's reactive power is also constrained by the corresponding inverter's rated capacity, modeled in eq. (14). For the safe and sustainable operation of the batteries, the energy B_j^t is constrained to be within some percentage limits of the rated battery SOC capacity, modeled using eq. (15).

4.2.3 ENApp-based MPDOPF with Batteries

Assuming the presence of a feasible solution for the MPCOPF problem, the MPDOPF is formulated by decomposing the distribution system into multiple small areas. In this paper, the interaction between the two areas will follow the principle of ENApp algorithm. The ENApp algorithm leverages the radial topology of the distribution network to solve the network-level optimization problem in a distributed manner. Each area has a local controller (LC) that solves its specific local optimization problem. The local optimization

problem will be the same MPOPF as described in Section II-B but defined using only the variables and parameters specific for the corresponding area. The boundary buses between two areas are accounted as voltage sources for downstream areas and load buses for upstream areas. By knowing the upstream voltage and downstream load data, the LCs will solve their area-specific MPOPF in parallel. Once LC problem converges, the downstream and upstream LCs inform power flows and voltage data to their respective upstream and downstream areas. The LCs will again solve their local MPOPF and exchange the updated boundary variables with their neighbors. This iterative process terminates after a convergence is achieved at all boundary buses. Comprehensive details of the ENApp algorithm are available in [31]. Note that for the case of multi-period optimization with T time steps, each area exchanges a data vector containing $2T$ boundary variables with its neighboring areas. This includes voltage and power flow data for each of the T time steps.

4.3 Case Study Demonstration: IEEE 123 Bus Test System

4.3.1 Test System Description

The case studies are conducted on the balanced three-phase version of the IEEE 123 bus test system, which has 85 Load Nodes. Additionally, 20% (17) and 30% (26) of these load nodes also contain reactive power controllable PVs and BESS, respectively. Their ratings are as per Table 3. To demonstrate the effectiveness of the proposed algorithm, the test system is divided into four areas as shown in Fig. 4. It is assumed that a horizon-wide forecast for loads p_L^t , solar power output p_D^t and cost of substation power C^t is available to the distribution system operator. Initially, the study is carried out for 5 hours with input data shown in Fig. 5. The five-hour workflow is described below.

4.3.2 Simulation Workflow

All simulations were set up in MATLAB 2023a including both the high level algorithms as well as calls to the optimization solver. MATLAB’s `fmincon` function was used to parse the nonlinear nonconvex optimization problem described by eqs. (4) to (15) in tandem with the SQP optimization algorithm to solve it. From the completed simulations, the resultant optimal control variables were obtained, and were passed through an OpenDSS engine (already configured with system data and forecast values) in order to check for the ACOPF feasibility of the results. The associated code may be found in [19]. As the IEEE 123 bus system is decomposed into 4 areas, so the total number of variables exchanged at each iteration for

Table 3: Parameter values

Parameter	Value
V_{min}, V_{max}	0.95 pu, 1.05 pu
$p_{D_{R_j}}$	$0.33p_{L_{R_j}}$
$S_{D_{R_j}}$	$1.2p_{D_{R_j}}$
$P_{B_{R_j}}$	$0.33p_{L_{R_j}}$
$S_{B_{R_j}}$	$1.2P_{B_{R_j}}$
B_{R_j}	$T_{fullCharge} \times P_{B_{R_j}}$
$T_{fullCharge}$	4 h
Δt	1 h
η_c, η_d	0.95, 0.95
soc_{min}, soc_{max}	0.30, 0.95
α	0.001

the 5-hour simulation of the MPDOPF is $2 * 3 * 5 = 30$.

4.4 Simulation Results and Performance Analysis

In the following subsections, the proposed MPDOPF algorithm is compared against the MPCOPF algorithm in terms of resultant optimal control variables, optimality gap in the objective function, and computational performance. Secondly, the resultant control variables are tested for ACOPF feasibility against OpenDSS. Section 4.4.1 describes the comparison over a 5 hour horizon with an additional focus on describing the workflow of the MPDOPF algorithm. Section 4.4.2 describes the comparison over a 10 hour horizon to test for the scalability of the MPDOPF algorithm.

4.4.1 5-Hour Horizon Results

Table 4 depicts a comparison between MPCOPF and MPDOPF in their problem scope, results and computational performance.

4.4.1.1 Largest Subproblem vs. Computational Performance This first section of the Table 4, ‘largest subproblem’ provides specifics of the ‘computational bottleneck’ encountered by either algorithm during its course. As described in Section 4.2.3, the bottleneck represents the OPF subproblem which is computationally the most intensive and thus is a

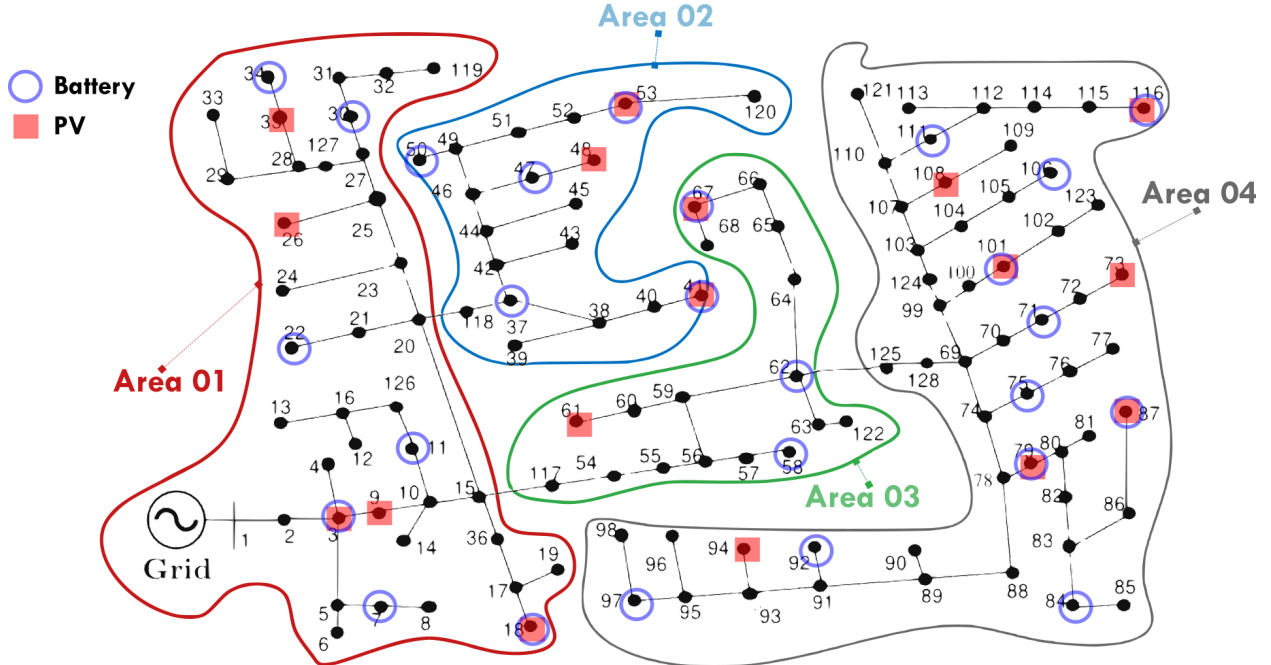


Figure 4: IEEE 123 node system divided into four areas

key indicator of the expected time the algorithm will take to complete. As can be seen in the third section ‘Computation’, there is more than a 10x speedup in computation time with MPDOPF, even though 5 such iterations were performed, totalling to 20 OPF calls over the 4 areas of the test system.

4.4.1.2 Optimality of Objective Function and Control Variables The second section of the Table 4 i.e. ‘Simulation results’ showcases that MPDOPF provides almost zero optimality gap (same values for Substation Power Cost, the objective function). Interestingly, there is a significant difference in the suggested optimal reactive power control values for inverters associated with DERs and batteries (results aggregated over all components over the horizon for conciseness). This highlights the fact that a nonconvex nonlinear optimization problem may not necessarily have a unique global optimal point. There is a possibility of having multiple feasible solutions with the same objective function value.

4.4.1.3 ACOPF Feasibility Analysis Table 5 showcases the ACOPF feasibility of the control values suggested by the MPDOPF algorithm. The first section ‘Full horizon’ describes the respective output variables for the entire horizon from MPDOPF and OpenDSS. The second section ‘Max. all-time discrepancy’ stores the highest discrepancy between key

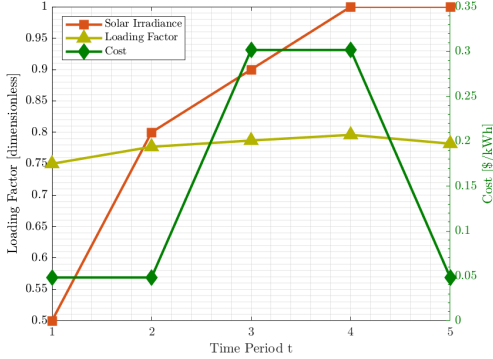


Figure 5: Forecasts for demand power, irradiance and cost of substation power over a 5 hour horizon

state/output variables for all components across any time between MPDOPF and OpenDSS. In both sections, the discrepancies are small enough to warrant the feasibility of the obtained solution.

Table 5: ACOPF feasibility analyses - 5 hour

Metric	MPDOPF	OpenDSS
Full horizon		
Substation real power (kW)	4308.14	4308.35
Line loss (kW)	76.12	76.09
Substation reactive power (kVAR)	656.24	652.49
Max. all-time discrepancy		
Voltage (pu)	0.0002	
Line loss (kW)	0.0139	
Substation power (kW)	0.3431	

To ensure that battery charging and discharging complementarity is respected without relying on integer constraints, the battery charging and discharging profiles were carefully examined. The results confirm this complementarity, as illustrated in Fig. 6 as one such example.

4.4.1.4 Workflow Analysis The workflow of the MPDOPF algorithm, which involves the exchange of boundary variables between parent-child area pairs, is illustrated in the convergence plots in Figs. 7 and 8. Each line graph represents a specific time period for both plots. Similarly, Fig. 9 shows the convergence of the objective function towards its optimal value over successive iterations. From these plots, we observe that although the

Table 4: Comparative analyses between MPCOPF and MPDOPF - 5 time-period horizon

Metric	MPCOPF	MPDOPF
Largest subproblem		
Decision variables	3150	1320
Linear constraints	5831	2451
Nonlinear constraints	635	265
Simulation results		
Substation power cost (\$)	576.31	576.30
Substation real power (kW)	4308.28	4308.14
Line loss (kW)	75.99	76.12
Substation reactive power (kVAR)	574.18	656.24
PV reactive power (kVAR)	116.92	160.64
Battery reactive power (kVAR)	202.73	76.01
Computation		
Number of Iterations	-	5
Total Simulation Time (s)	521.25	49.87

decision variables may initially deviate from their optimal values, they gradually approach optimality with each rolling iteration, converging after 5 macro iterations in this instance.

4.4.2 10-Hour Horizon: Scalability Analysis

To demonstrate the scalability of the proposed algorithm, additional simulations were conducted over a 10-hour time horizon. Fig. 10 shows the forecasted profiles for load, solar irradiance and cost of substation power over the 10-hour horizon. The simulation results are summarized in Tables 6 and 7.

From the comparison against MPCOPF in Table 6, it can again be seen that MPDOPF is able to converge to the same optimal solution as MPCOPF. The computational speed up is even more pronounced than for the 5 time-period simulation. It was observed that the solution time for MPCOPF increased significantly with the length of the study horizon, whereas the increase in solution time for MPDOPF was comparatively smaller. This indicates that the proposed spatially distributed MPOPF framework is scalable to a certain extent.

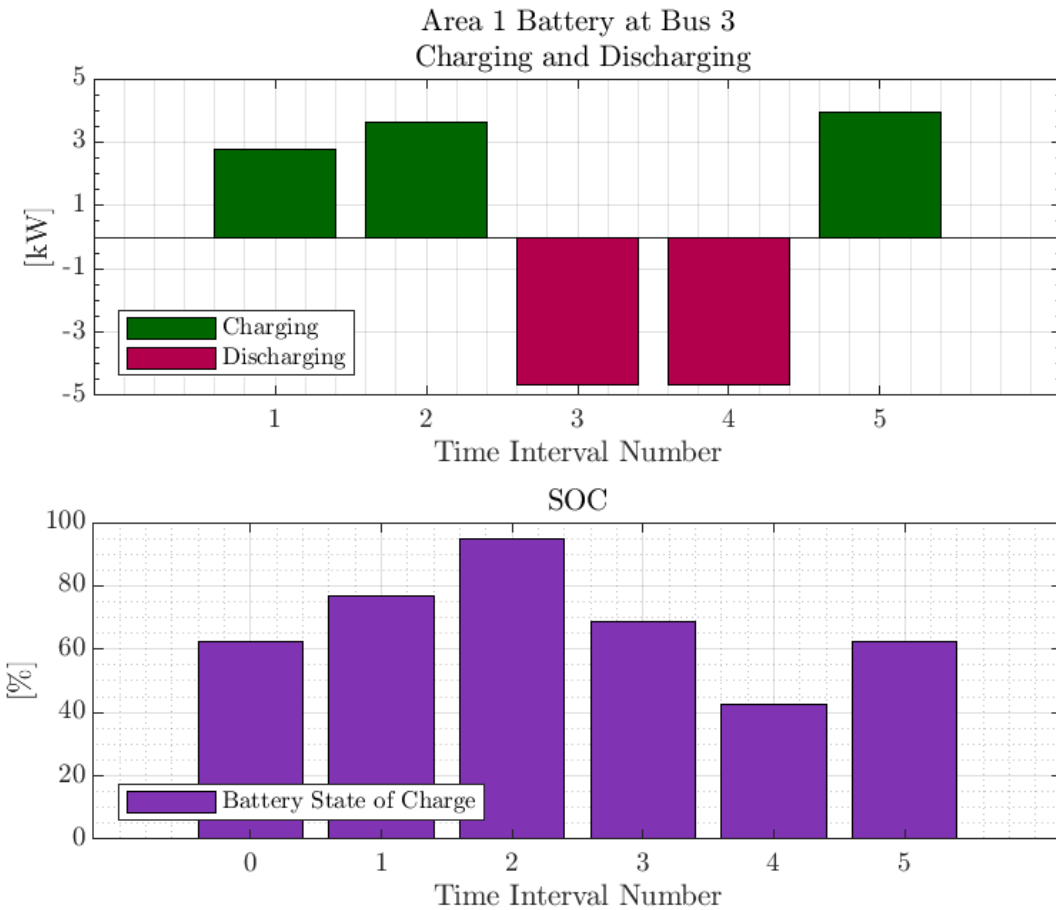


Figure 6: Charging-discharging and SOC graphs for battery at bus 3 located in Area 1 obtained by MPDOPF

Table 6: Comparison between MPCOPF and MPDOPF - 10 hour

Metric	MPCOPF	MPDOPF
Largest subproblem		
Decision variables	6300	2640
Linear constraints	11636	4891
Nonlinear constraints	1270	530
Simulation results		
Substation power cost (\$)	1197.87	1197.87
Substation real power (kW)	8544.28	8544.04
Line loss (kW)	148.67	148.94
Substation reactive power (kVAR)	1092.39	1252.03
PV reactive power (kVAR)	222.59	139.81
Battery reactive power (kVAR)	388.52	310.94
Computation	25	
Number of Iterations	-	5
Total Simulation Time (s)	4620.73	358.69

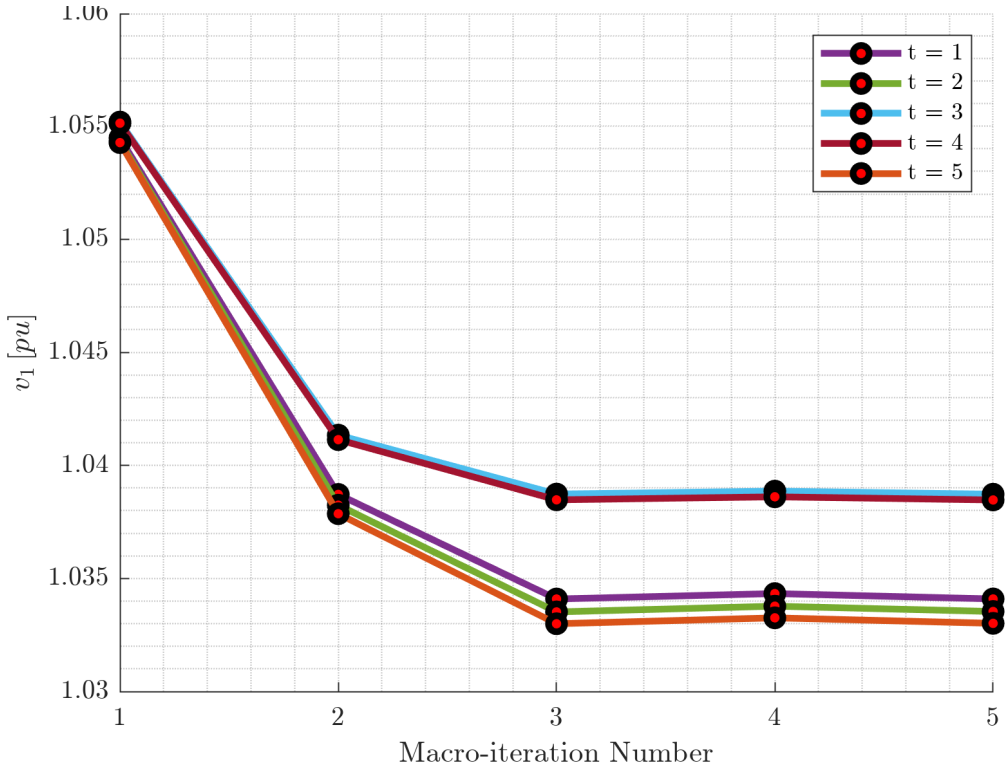


Figure 7: Shared voltage data from Area 1 to Area 2.

Again, as can be seen in Table 7 comparison against OpenDSS has yielded small discrepancies, attesting to the feasibility of the solution.

4.5 Summary and Discussion

The Equivalent Network Approximation (ENApp) approach provides an effective spatial decomposition framework for solving multi-period optimal power flow problems with energy storage in distribution networks. The key advantages of this approach include:

- **Computational Efficiency:** The MPDOPF algorithm achieves more than 10x speedup compared to centralized MPCOPF for medium-sized networks, with the advantage increasing for longer time horizons
- **Scalability:** The computational complexity grows more favorably with network size and time horizon length compared to centralized approaches
- **Distributed Architecture:** Each area solves its local optimization problem inde-

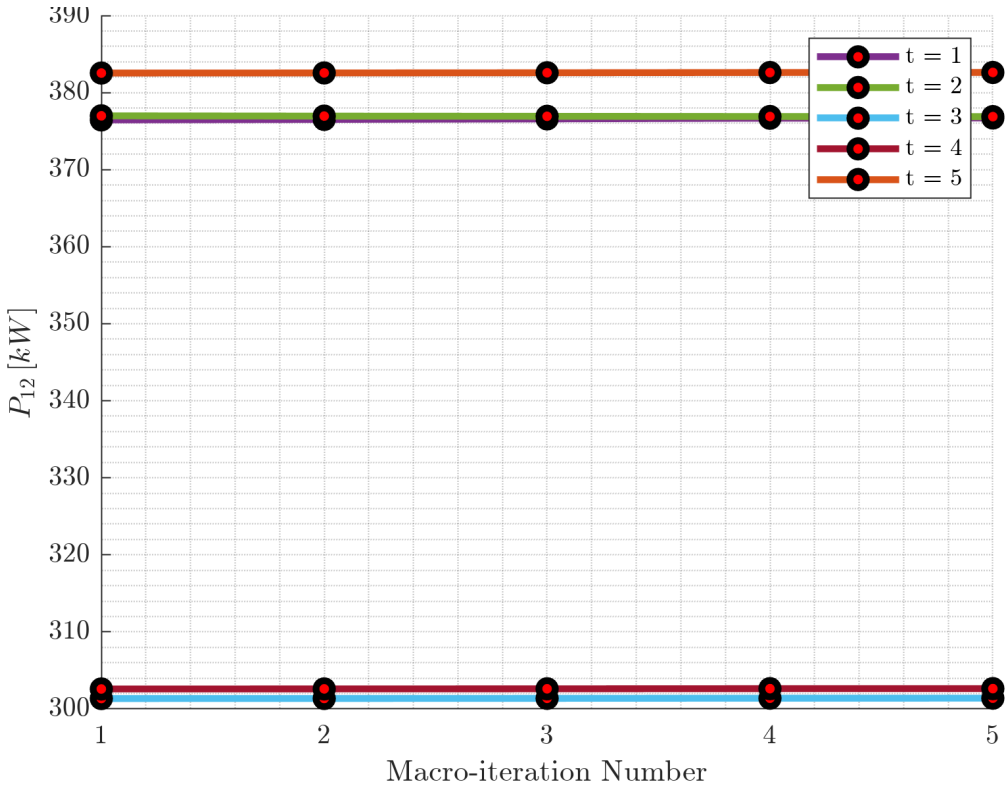


Figure 8: Shared real power data from Area 4 into Area 2.

pendently, enabling parallel computation and reducing the need for centralized data aggregation

- **Solution Quality:** The MPDOPF converges to the same optimal objective value as MPCOPF, with negligible optimality gap
- **ACOPF Feasibility:** The solutions obtained from MPDOPF are validated against OpenDSS, showing excellent agreement with acceptable discrepancies

The numerical results on the IEEE 123 bus system demonstrate that ENApp successfully decomposes the spatial network constraints while handling temporal coupling through battery SOC dynamics. The algorithm converges within a few macro iterations (typically 5), and the final solution matches the centralized optimal solution within the specified tolerances. The ACOPF feasibility analysis confirms that the obtained control variables can be implemented in practice with minimal deviation from the desired operating point.

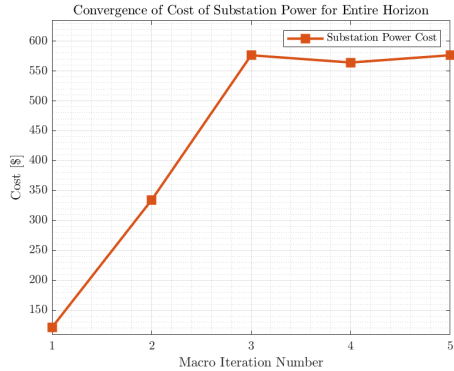


Figure 9: Convergence of objective function value with each MPDOPF iteration

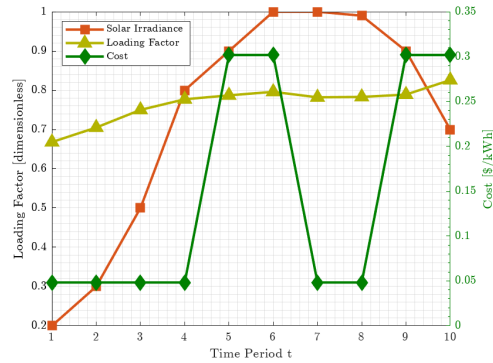


Figure 10: Forecasts for demand power, irradiance and cost of substation power over a 10 hour Horizon

4.5.1 Key Observations

Several important observations emerge from the case study results:

- 1. Multiple Optimal Solutions:** The nonconvex nature of the MPOPF problem results in multiple feasible solutions with the same objective function value. This is evidenced by the different reactive power dispatch strategies between MPCOPF and MPDOPF, despite achieving the same cost.
- 2. Boundary Variable Convergence:** The convergence plots show smooth and monotonic convergence of boundary variables (voltage and power flow) across area boundaries, indicating stable numerical behavior of the ENApp algorithm.
- 3. Battery Complementarity:** The battery loss cost term successfully prevents simul-

Table 7: ACOPF feasibility analyses - 10 hour

Metric	MPDOPF	OpenDSS
Full horizon		
Substation real power (kW)	8544.04	8544.40
Line loss (kW)	148.94	148.87
Substation reactive power (kVAR)	1252.03	1243.36
Max. all-time discrepancy		
Voltage (pu)	0.0002	
Line loss (kW)	0.0132	
Substation power (kW)	0.4002	

taneous charging and discharging without requiring integer variables, simplifying the optimization problem while maintaining physical consistency.

4. **Scalability Advantage:** The computational advantage of MPDOPF becomes more pronounced as the problem size increases (from 5-hour to 10-hour horizon), demonstrating favorable scaling properties.

4.5.2 Implementation Status and Future Work

The ENApp-based MPDOPF framework has been successfully implemented and validated on the IEEE 123 bus test system with realistic DER and battery penetrations. The current implementation uses the branch flow model with nonlinear constraints, solved using sequential quadratic programming (SQP) within MATLAB’s `fmincon` solver.

Scalability Limitations: While ENApp achieves 10-13× speedup via spatial decomposition, computational challenges remain for *long time horizons* (e.g., $T > 10$ hours). The coupling across all time periods within each spatial subproblem still requires solving large-scale optimization problems. For planning horizons spanning 24+ hours, spatial decomposition alone proves insufficient. This motivates the need for *temporal decomposition* strategies—the focus of the next chapter—which decompose the time horizon into manageable sub-horizons while maintaining feasibility and near-optimality.

Future extensions of this work will focus on:

- **Larger Networks:** Applying MPDOPF to larger distribution networks (e.g., IEEE 8500 bus system) to further validate scalability
- **Higher DER Penetrations:** Testing the algorithm with increased renewable energy and battery penetrations (e.g., 50% PV, 50% BESS)

- **Combined Decomposition:** Integrating spatial (ENApp) and temporal (tADMM) decomposition techniques for enhanced scalability in large-scale, long-horizon problems
- **Convergence Acceleration:** Investigating adaptive parameter tuning and warm-start strategies to reduce the number of macro iterations

The successful demonstration of ENApp-based MPDOPF on realistic test cases provides a strong foundation for deploying distributed optimization algorithms in operational settings. However, recognizing the complementary need for temporal decomposition leads naturally to the investigation presented in the following chapter.

5 Temporal Decomposition via Differential Dynamic Programming

5.1 Introduction

While the spatial decomposition approach (ENApp) demonstrated in Section 4 effectively partitions the network topology, it encounters computational challenges for long time horizons due to the temporal coupling through battery state-of-charge (SOC) dynamics. As shown in the previous chapter, spatial decomposition alone remains computationally expensive for planning horizons exceeding 10 hours.

This motivates the investigation of **temporal decomposition** methods that can break down the multi-period optimization problem across time while maintaining feasibility and near-optimality. One such approach is **Differential Dynamic Programming (DDP)** [3], which leverages the sequential structure of the MPOPF problem to decompose it into a backward-forward sweep algorithm.

DDP offers several advantages for MPOPF:

- **Temporal Decomposition:** Solves single-period subproblems sequentially
- **Handles Nonlinearity:** Can work with nonlinear branch flow models (BFM-NL) without requiring linearization
- **Scalability:** Computational complexity grows linearly with time horizon length
- **Local Optimality:** Guarantees convergence to local optima through iterative refinement
- **Guaranteed Feasibility always:** At any Forward Pass iteration ensures that its current solution is feasible (provided there are no terminal constraints on state variable such as terminal SOC constraint)

5.2 DDP Algorithm for MPOPF

The DDP algorithm iteratively refines a nominal trajectory through backward-forward sweeps. For MPOPF, the algorithm proceeds as follows:

DDP Workflow: Forward Pass for Non-Terminal Time-Step $t \in \{1, 2, \dots, T-1\}$

At each non-terminal time-step, the forward pass solves the following optimization problem where the previous battery SOC B_j^{t-1} is known from the previous time-step, and the Lagrange multiplier $\mu_{SOC_j}^{t+1}$ from the next time-step influences the current decision:

$$\min \quad C^t P_{Subs}^t \quad (16)$$

$$\begin{aligned} & + \alpha \sum_{j \in \mathcal{B}} \left\{ (1 - \eta_c) P_{c_j}^t + \left(\frac{1}{\eta_d} - 1 \right) P_{d_j}^t \right\} \\ & + \sum_{j \in \mathcal{B}} \mu_{SOC_j}^{t+1} \{ -B_j^t \} \end{aligned}$$

s.t.

$$0 = \sum_{(j,k) \in \mathcal{L}} \{ P_{jk}^t \} - \{ P_{ij}^t - r_{ij} l_{ij}^t \} - (P_{d_j}^t - P_{c_j}^t) - (p_{Dj}^t) + p_{Lj}^t \quad (17)$$

$$0 = \sum_{(j,k) \in \mathcal{L}} \{ Q_{jk}^t \} - \{ Q_{ij}^t - x_{ij} l_{ij}^t \} - (q_{Dj}^t) - (q_{B_j}^t) + q_{Lj}^t \quad (18)$$

$$0 = v_i^t - v_j^t - 2(r_{ij} P_{ij}^t + x_{ij} Q_{ij}^t) + \{ r_{ij}^2 + x_{ij}^2 \} l_{ij}^t \quad (19)$$

$$0 = (P_{ij}^t)^2 + (Q_{ij}^t)^2 - v_i^t l_{ij}^t \quad (20)$$

$$0 = B_j^t - \left\{ B_j^{t-1} + \Delta t \eta_c P_{c_j}^t - \Delta t \frac{1}{\eta_d} P_{d_j}^t \right\} \quad (21)$$

$$0 \geq B_{min_j}^t - B_j^t \quad (22)$$

$$0 \geq B_j^t - B_{Max_j}^t \quad (23)$$

$$0 \geq \text{All other inequality constraints} \quad (24)$$

DDP Workflow: Forward Pass for the Terminal Time-Step $t = T$

At the terminal time-step, the forward pass includes the terminal penalty on battery SOC deviation from reference:

$$\begin{aligned}
\min \quad & C^t P_{Subs}^t \\
& + \alpha \sum_{j \in \mathcal{B}} \left\{ (1 - \eta_c) P_{c_j}^t + \left(\frac{1}{\eta_d} - 1 \right) P_{d_j}^t \right\} \\
& + \gamma \sum_{j \in \mathcal{B}} \left\{ (B_j^T - B_{ref_j})^2 \right\}
\end{aligned} \tag{25}$$

s.t.

$$0 = \sum_{(j,k) \in \mathcal{L}} \{P_{jk}^t\} - \{P_{ij}^t - r_{ij} l_{ij}^t\} - (P_{d_j}^t - P_{c_j}^t) - (p_{Dj}^t) + p_{Lj}^t \tag{26}$$

$$0 = \sum_{(j,k) \in \mathcal{L}} \{Q_{jk}^t\} - \{Q_{ij}^t - x_{ij} l_{ij}^t\} - (q_{Dj}^t) - (q_{Bj}^t) + q_{Lj}^t \tag{27}$$

$$0 = v_i^t - v_j^t - 2(r_{ij} P_{ij}^t + x_{ij} Q_{ij}^t) + \{r_{ij}^2 + x_{ij}^2\} l_{ij}^t \tag{28}$$

$$0 = (P_{ij}^t)^2 + (Q_{ij}^t)^2 - v_i^t l_{ij}^t \tag{29}$$

$$0 = B_j^t - \left\{ \textcolor{red}{B_j^{t-1}} + \Delta t \eta_c P_{c_j}^t - \Delta t \frac{1}{\eta_d} P_{d_j}^t \right\} \tag{30}$$

$$0 \geq B_{min_j}^t - B_j^t \tag{31}$$

$$0 \geq B_j^t - B_{Max_j}^t \tag{32}$$

$$0 \geq \text{All other inequality constraints} \tag{33}$$

5.3 Computational Advantages for Long-Horizon MPOPF

DDP offers significant computational benefits compared to monolithic MPOPF formulations:

1. **Parallelizable Forward Pass:** Subproblems within forward pass can be solved in parallel across time steps.
2. **Handles Nonlinearity:** Works directly with BFM-NL [13] without requiring convex relaxations or linear approximations that may sacrifice accuracy.
3. **Warm Starting:** Previous solutions provide excellent initialization for rolling-horizon Model Predictive Control (MPC) implementations.

For MPOPF, the projection approach is most practical, as it maintains power flow feasibility explicitly.

5.4 Relationship to Other Decomposition Methods

DDP provides complementary capabilities to the spatial decomposition (ENApp, Section 4):

- **ENApp:** Decomposes across *space* (network topology), coupling through boundary voltage and power variables
- **DDP:** Decomposes across *time* (temporal horizon), coupling through battery SOC evolution
- **Combined Approach:** Apply spatial decomposition (ENApp) within each DDP time-step subproblem, achieving both spatial and temporal scalability

Compared to ADMM-based temporal decomposition (next chapter):

- **DDP:** Sequential backward-forward sweeps, local convergence to stationary points, guaranteed feasible solution at any stage of the algorithm
- **tADMM:** Parallel consensus-based optimization, handles separable structure, global convergence guarantees for convex problems, no guarantee of feasible solution at any current algorithm stage
- **Trade-off:** DDP more efficient for few iterations (warm start), ADMM more parallelizable for cold start

5.5 Numerical Results: 24-Hour Horizon on IEEE 123-Bus System

To demonstrate the effectiveness of DDP for temporal decomposition, we present results for a 24-hour planning horizon on the IEEE 123-bus single-phase equivalent system with 20% PV penetration (31% of buses with batteries). The system is optimized using the nonlinear Branch Flow Model (BFM-NL) with Ipopt solver.

5.5.1 System Configuration and Convergence

Figure 11 shows the forecast curves for load, PV generation, and electricity cost over the 24-hour horizon. The load exhibits typical residential patterns with morning and evening peaks. PV generation follows solar irradiance with peak output during midday hours. Electricity costs vary throughout the day, with higher prices during peak demand periods.

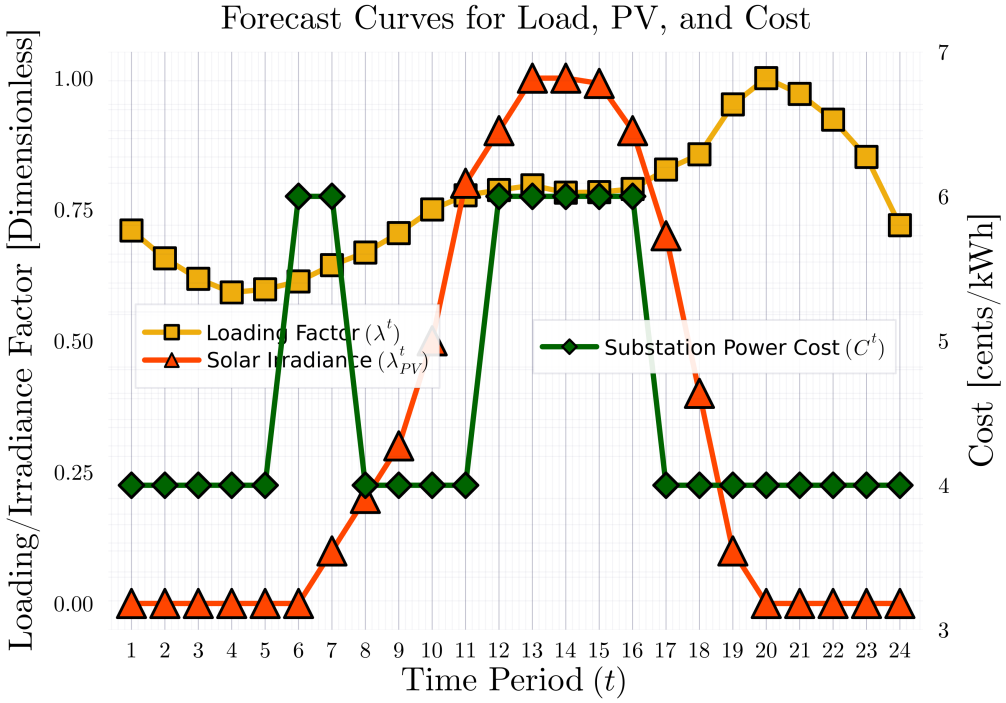


Figure 11: Forecast curves for loading factor (λ^t), solar irradiance (λ_{PV}^t), and substation power cost (C^t) over the 24-hour horizon.

Figures 12 and 13 present the convergence behavior of DDP compared to the temporally brute-forced (monolithic) approach for both BFM-NL and LinDistFlow models. The DDP algorithm demonstrates rapid convergence, achieving near-optimal solutions within 4-5 forward passes. After this initial rapid descent phase, the algorithm continues to refine the solution through additional iterations.

To further validate the robustness of DDP across different loading scenarios, additional tests were performed on a modified IEEE 123-bus variant (ieee123B) with different load profiles. Figures 14 and 15 show the convergence behavior for this system configuration.

Key observations from the convergence behavior:

- **Rapid Initial Convergence:** DDP achieves near-optimal cost within 4-5 forward passes, significantly faster than iterative ADMM-based methods
- **Model Independence:** Both BFM-NL and LinDistFlow exhibit similar convergence patterns, validating DDP's applicability across different power flow models
- **System Robustness:** DDP performs consistently well across both ieee123A and

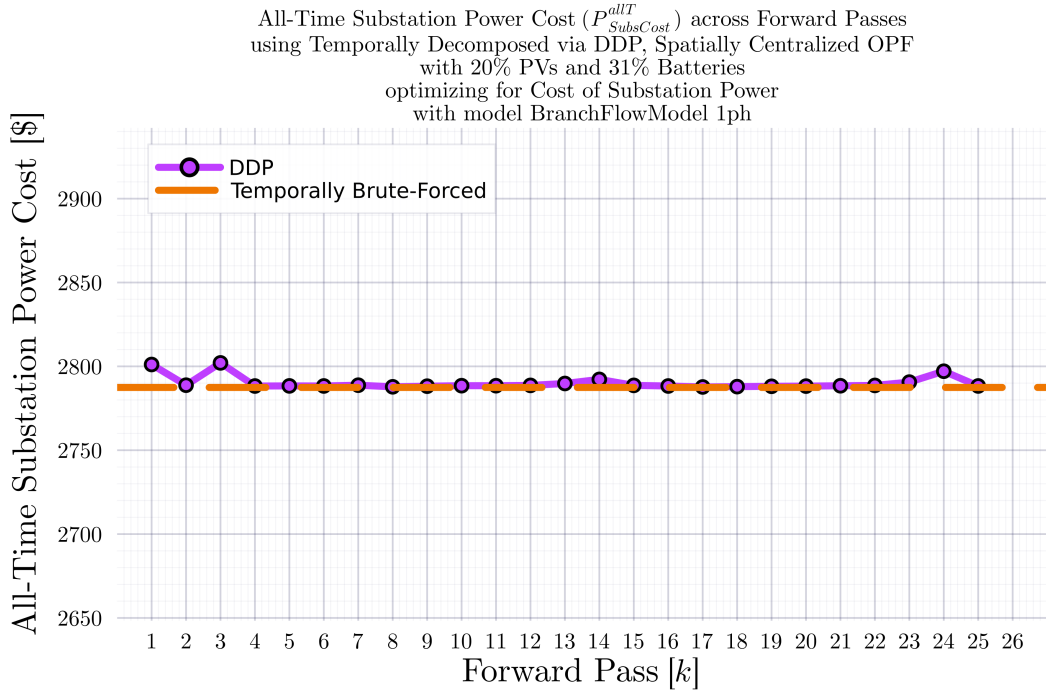


Figure 12: All-time substation power cost convergence across forward passes using temporally decomposed DDP with spatially centralized formulation. BFM-NL model with 20% PVs and 31% batteries. DDP converges to the brute-forced solution within 4-5 iterations.

ieee123B system variants with different loading profiles, demonstrating robustness to system parameters

- **Optimality Gap:** After convergence, DDP maintains costs very close to the brute-forced (monolithic) solution, with differences less than 0.1%

5.5.2 Performance Summary

The final converged solution for ieee123A (after 26 forward passes) achieved the performance metrics summarized in Table 8. DDP performed similarly well on ieee123B, confirming the algorithm’s effectiveness across different system configurations.

Key observations from Table 8:

- **High Accuracy:** Voltage discrepancies below 0.08% and power discrepancies less than 1% of peak power validate the solution quality

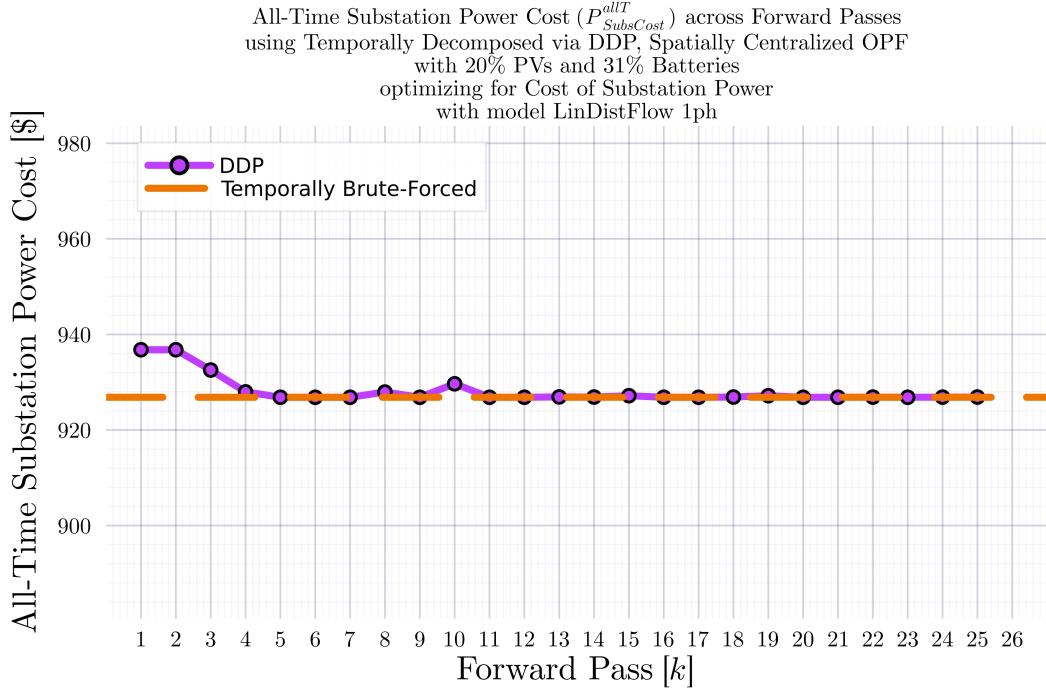


Figure 13: All-time substation power cost convergence across forward passes using temporally decomposed DDP with spatially centralized formulation. LinDistFlow model with 20% PVs and 31% batteries. Similar rapid convergence observed with the linear model.

- **Effective DER Coordination:** Batteries perform significant transactions (1,034 kW total) while maintaining reasonable final SOC deviation
- **Computational Efficiency:** Achieving these results through temporal decomposition enables scalability to longer horizons

5.5.3 Preliminary Results on Larger Systems

To explore DDP’s scalability to larger distribution networks, preliminary tests were conducted on the IEEE 730-bus system. Figure 16 shows the convergence behavior using LinDistFlow with relaxed convergence criteria (function value-based termination).

While the results in Figure 16 demonstrate that DDP’s optimization trajectory is moving in the right direction, the convergence behavior suggests that further research is needed to:

- **Enhance Convergence Rigor:** Develop more robust stopping criteria and regularization strategies for larger systems

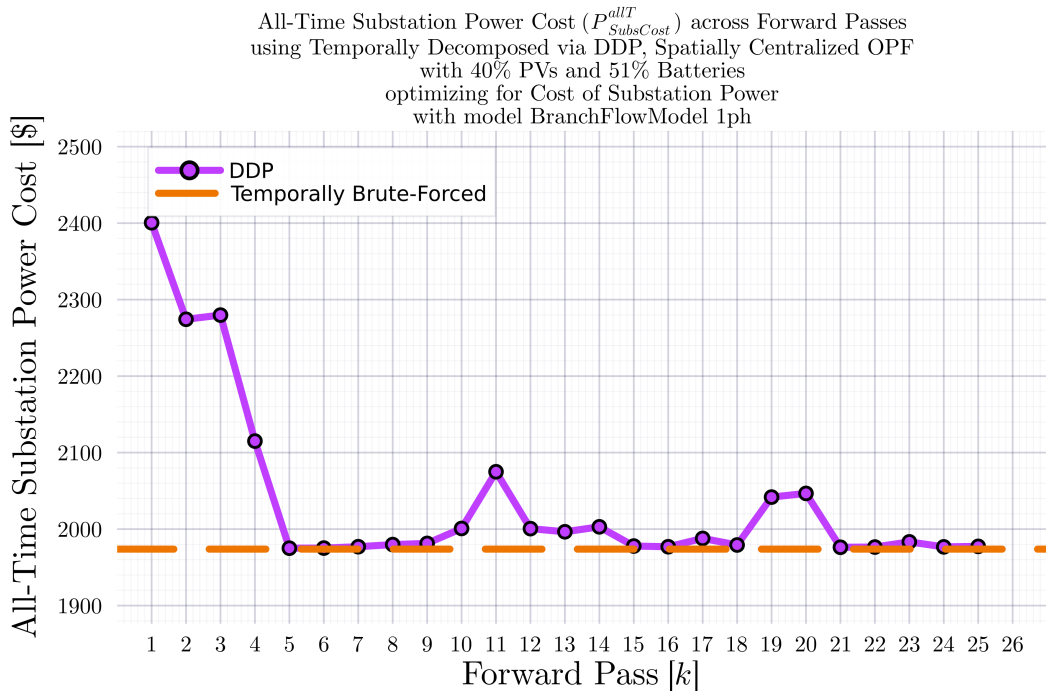


Figure 14: All-time substation power cost convergence for ieee123B system using DDP with BFM-NL model. The algorithm exhibits similar rapid convergence characteristics, demonstrating robustness across different system configurations.

- **Improve Numerical Stability:** Investigate adaptive step-sizing and line-search methods tailored to large-scale MPOPF
- **Scale Initialization:** Develop better warm-start strategies that leverage system structure for networks with 500+ buses

These preliminary findings indicate that while DDP shows promise for temporal decomposition of large-scale MPOPF problems, additional algorithmic development is necessary to achieve the same level of convergence reliability observed on smaller systems (ieee123A/B). This represents an important direction for future work.

5.6 Summary

Differential Dynamic Programming provides a principled temporal decomposition framework for large-scale MPOPF problems. By reformulating MPOPF as an optimal control problem with battery SOC as states, DDP achieves:

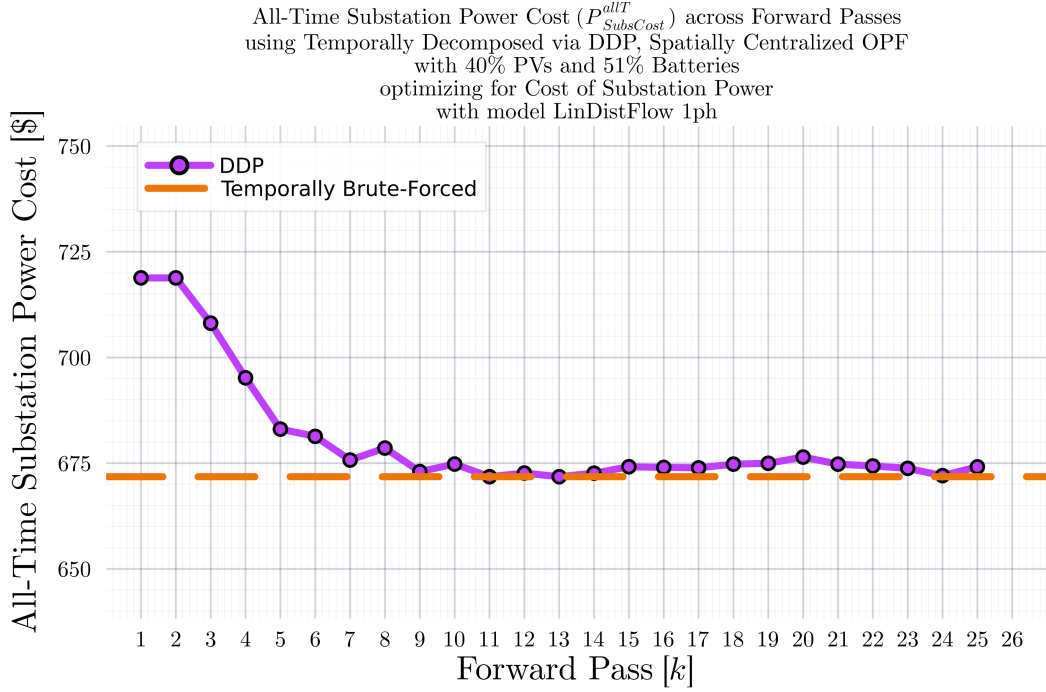


Figure 15: All-time substation power cost convergence for ieee123B system using DDP with LinDistFlow model. Consistent convergence behavior validates DDP’s effectiveness across both power flow formulations and system variants.

- **Linear time complexity** $\mathcal{O}(N)$ in horizon length N
- **Natural handling** of nonlinear branch flow models (BFM-NL) without approximation
- **Sequential structure** exploiting causal battery dynamics
- **Warm-start capability** for rolling-horizon MPC implementations

The key insight is that battery SOC couples time periods, while power flow constraints decouple across time. DDP leverages this structure by solving backward-forward passes, where:

- **Backward pass:** Computes optimal feedback policy (how battery should react to SOC deviations)
- **Forward pass:** Rolls out trajectory respecting power flow constraints at each time step

Table 8: DDP Performance Summary for 24-Hour Horizon on IEEE 123-Bus System with 20% PV and 31% Battery Penetration (BFM-NL Model, Ipopt Solver)

Category	Metric	Value
Economic & Power Flow	Total Substation Power Cost	\$944.35
	Total Line Loss	390.35 kW
	Peak Substation Power	1,192.95 kW
	Total Substation Power	21,022.04 kW + 7,232.8 kVAr
DER Performance	PV Generation (Total)	607.46 kW + 1,972.4 kVAr
	Battery Net Discharge	118.29 kW + 3,310.45 kVAr
	Battery Transaction Magnitude	1,034.31 kW
	Final SOC Deviation from Reference	171.32 kWh
Solution Quality	Maximum Voltage Discrepancy	0.000759 pu
	Maximum Line Loss Discrepancy	13.15 kW
	Maximum Substation Power Discrepancy	13.10 kW, 14.48 kVAr

While DDP demonstrates strong theoretical properties for nonlinear optimal control, its practical performance for MPOPF depends on:

1. Quality of initialization (warm start from previous solution or LinDistFlow approximation)
2. Constraint handling method (projection onto feasible set most effective)
3. Regularization tuning (ensuring Q_{uu} invertibility without over-damping)

The next chapter explores an alternative temporal decomposition approach based on ADMM consensus, which trades off the Markov exploitation of DDP for greater parallelizability and convex convergence guarantees.

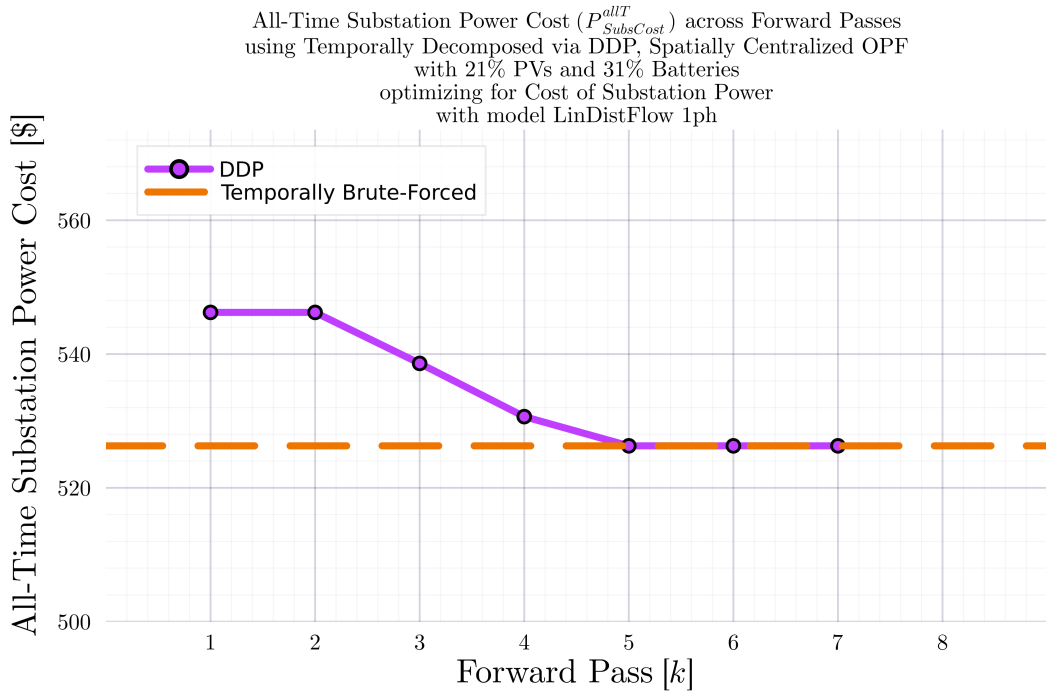


Figure 16: All-time substation power cost convergence for IEEE 730-bus system using DDP with LinDistFlow model. The algorithm shows directional convergence toward the optimal solution, though requiring relaxed termination criteria. Results indicate DDP's potential for large-scale systems while highlighting areas for algorithmic refinement.

6 Temporal Decomposition via Temporal Alternating Direction Method of Multipliers (tADMM)

6.1 Introduction and Motivation

Multi-period optimal power flow (MPOPF) problems are computationally challenging due to the coupling of variables across time periods through energy storage devices, such as batteries. The temporal coupling arises from the state-of-charge (SOC) dynamics, which link the battery's energy level at each time step to its charging/discharging decisions throughout the entire planning horizon. For large-scale distribution networks with multiple time periods, solving the centralized MPOPF problem becomes intractable.

The Alternating Direction Method of Multipliers (ADMM) is a powerful decomposition technique for solving large-scale convex optimization problems [36, 37]. ADMM is particularly effective for problems that can be decomposed into smaller, more manageable subproblems. The temporal ADMM (tADMM) approach adapts the classical ADMM framework to decompose the MPOPF problem across the temporal dimension, enabling parallel computation of individual time-step subproblems while maintaining consensus on the battery SOC trajectories.

The key insight of tADMM is that while spatial network constraints (power flow equations, voltage limits) are local to each time step, the temporal coupling through battery SOC can be handled through consensus variables. Each time-step subproblem maintains its own local copy of the battery SOC trajectory, and these local copies are coordinated through a global consensus variable that is updated iteratively. This decomposition structure allows for:

- **Parallel computation:** Each time-step subproblem can be solved independently and in parallel
- **Scalability:** Computational complexity grows more favorably with the number of time periods compared to centralized approaches
- **Modularity:** The framework can accommodate different network models (LinDist-Flow, copper plate) without changing the decomposition structure

6.2 LinDistFlow MPOPF with tADMM

6.2.1 Problem Overview

The Temporal ADMM (tADMM) algorithm decomposes the multi-period optimal power flow problem for distribution networks into T subproblems, each corresponding to one time period. This formulation uses the linearized DistFlow model to capture network physics including voltage drops and reactive power flows. The algorithm maintains consensus on battery state-of-charge (SOC) trajectories across all subproblems through an iterative update procedure.

6.2.2 Variable Color Coding

To clearly distinguish the different types of variables in the tADMM formulation, we use the following color-coding scheme:

- $\mathbf{B}_j^{t_0}[t]$ (Blue): Local SOC variables for battery j in subproblem t_0 , evaluated at time t . These are the primal variables optimized in each subproblem.
- $\hat{\mathbf{B}}_j[t]$ (Red): Global consensus SOC for battery j at time t . This represents the agreed-upon SOC trajectory that all subproblems aim to converge to.
- $\mathbf{u}_j^{t_0}[t]$ (Green): Local scaled dual variables for battery j in subproblem t_0 , for time t . These accumulate the consensus violation and guide convergence.

6.2.3 Sets and Indices

- \mathcal{N} : Set of all nodes (buses)
- \mathcal{L} : Set of all branches (lines)
- \mathcal{L}_1 : Set of branches connected to substation (node 1)
- \mathcal{B} : Set of nodes with batteries
- \mathcal{D} : Set of nodes with PV (DER)
- $\mathcal{T} = \{1, 2, \dots, T\}$: Set of time periods
- $t_0 \in \mathcal{T}$: Index for a specific time period in tADMM decomposition

- $j \in \mathcal{N}$: Node index
- $(i, j) \in \mathcal{L}$: Branch from node i to node j

6.2.4 tADMM Algorithm Structure

The tADMM algorithm follows the consensus-based ADMM framework [36, 37], where the true global problem involves a single consensus variable that is used (partially or fully) by all individual subproblems. In the context of MPOPF, the consensus variable is the battery SOC trajectory, and each time-step subproblem maintains its own local copy of this trajectory.

The algorithm alternates between three update steps at each iteration k :

6.2.4.1 Step 1: Subproblem Update (Blue Variables) In the first update step, we solve each subproblem $t_0 \in \{1, 2, \dots, T\}$ independently and in parallel. Each subproblem optimizes its local copy of the battery SOC trajectory $\mathbf{B}_j^{\text{to}}[\mathbf{t}]$ along with the network variables for its specific time step. The latest values of the global consensus variable $\hat{\mathbf{B}}_j[\mathbf{t}]$ and dual variables $\mathbf{u}_j^{\text{to}}[\mathbf{t}]$ from the previous iteration are used to guide the optimization toward consensus.

For each subproblem $t_0 \in \{1, 2, \dots, T\}$:

$$\begin{aligned} & \min_{\substack{P_{\text{Subs}}^{t_0}, Q_{\text{Subs}}^{t_0}, \\ P_{ij}^{t_0}, Q_{ij}^{t_0}, v_j^{t_0}, q_{D,j}^{t_0, \\ P_{B,j}^t, \mathbf{B}_j^{\text{to}}[\mathbf{t}], \\ \forall j \in \mathcal{B}, t \in \mathcal{T}}} c^{t_0} \cdot P_{\text{Subs}}^{t_0} \cdot P_{\text{BASE}} \cdot \Delta t + C_B \sum_{j \in \mathcal{B}} (P_{B,j}^{t_0})^2 \cdot P_{\text{BASE}}^2 \cdot \Delta t \\ & + \frac{\rho}{2} \sum_{j \in \mathcal{B}} \sum_{t=1}^T \left(\mathbf{B}_j^{\text{to}}[\mathbf{t}] - \hat{\mathbf{B}}_j[\mathbf{t}] + \mathbf{u}_j^{\text{to}}[\mathbf{t}] \right)^2 \end{aligned} \quad (34)$$

Subject to:

Spatial Network Constraints (only for time t_0):

$$\text{Real power balance (substation): } P_{\text{Subs}}^{t_0} - \sum_{(1,j) \in \mathcal{L}_1} P_{1j}^{t_0} = 0 \quad (35)$$

$$\begin{aligned} \text{Real power balance (nodes): } P_{ij}^{t_0} - \sum_{(j,k) \in \mathcal{L}} P_{jk}^{t_0} &= P_{B,j}^{t_0} + p_{D,j}^{t_0} - p_{L,j}^{t_0}, \\ &\forall (i, j) \in \mathcal{L}, \end{aligned} \quad (36)$$

$$\text{Reactive power balance (substation): } Q_{\text{Subs}}^{t_0} - \sum_{(1,j) \in \mathcal{L}_1} Q_{1j}^{t_0} = 0 \quad (37)$$

$$\begin{aligned} \text{Reactive power balance (nodes): } Q_{ij}^{t_0} - \sum_{(j,k) \in \mathcal{L}} Q_{jk}^{t_0} &= q_{D,j}^{t_0} - q_{L,j}^{t_0}, \\ &\forall (i, j) \in \mathcal{L}, \end{aligned} \quad (38)$$

$$\text{KVL constraints: } v_i^{t_0} - v_j^{t_0} = 2(r_{ij}P_{ij}^{t_0} + x_{ij}Q_{ij}^{t_0}), \quad \forall (i, j) \in \mathcal{L} \quad (39)$$

$$\text{Voltage limits: } (V_{\min,j})^2 \leq v_j^{t_0} \leq (V_{\max,j})^2, \quad \forall j \in \mathcal{N} \quad (40)$$

$$\begin{aligned} \text{PV reactive limits: } -\sqrt{(S_{D,j})^2 - (p_{D,j}^{t_0})^2} &\leq q_{D,j}^{t_0} \leq \sqrt{(S_{D,j})^2 - (p_{D,j}^{t_0})^2}, \\ &\forall j \in \mathcal{D} \end{aligned} \quad (41)$$

Temporal Battery Constraints (entire horizon $t \in \{1, \dots, T\}$):

$$\text{Initial SOC: } \mathbf{B}_j^{\text{to}}[\mathbf{1}] = B_{0,j} - P_{B,j}^1 \cdot \Delta t, \quad \forall j \in \mathcal{B} \quad (42)$$

$$\text{SOC trajectory: } \mathbf{B}_j^{\text{to}}[\mathbf{t}] = \mathbf{B}_j^{\text{to}}[\mathbf{t-1}] - P_{B,j}^t \cdot \Delta t, \quad \forall t \in \{2, \dots, T\}, j \in \mathcal{B} \quad (43)$$

$$\begin{aligned} \text{SOC limits: } \text{SOC}_{\min,j} \cdot B_{\text{rated},j} &\leq \mathbf{B}_j^{\text{to}}[\mathbf{t}] \leq \text{SOC}_{\max,j} \cdot B_{\text{rated},j}, \\ &\forall t \in \mathcal{T}, j \in \mathcal{B} \end{aligned} \quad (44)$$

$$\text{Power limits: } -P_{B,\text{rated},j} \leq P_{B,j}^t \leq P_{B,\text{rated},j}, \quad \forall t \in \mathcal{T}, j \in \mathcal{B} \quad (45)$$

Key Formulation Notes:

- **Network variables** ($P_{\text{Subs}}^{t_0}, Q_{\text{Subs}}^{t_0}, P_{ij}^{t_0}, Q_{ij}^{t_0}, v_j^{t_0}, q_{D,j}^{t_0}$) are optimized *only* for time step t_0 , representing the spatial network state at that particular time
- **Battery power** $P_{B,j}^t$ is optimized for the *entire* horizon $t \in \{1, \dots, T\}$ to allow proper accounting of temporal coupling
- **Local SOC trajectory** $\mathbf{B}_j^{\text{to}}[\mathbf{t}]$ is computed for *all* time steps $t \in \{1, \dots, T\}$ based on the battery power decisions

- The ADMM consensus penalty compares the full local trajectory $\mathbf{B}_j^{\text{to}}[\mathbf{t}]$ with the global master copy $\hat{\mathbf{B}}_j[\mathbf{t}]$, penalized by the dual variables $\mathbf{u}_j^{\text{to}}[\mathbf{t}]$
- Each battery $j \in \mathcal{B}$ has its own set of local/global SOC variables and dual variables

6.2.4.2 Step 2: Consensus Update (Red Variables) After all subproblems have been solved in parallel to obtain the latest values of $\mathbf{B}_j^{\text{to}}[\mathbf{t}]$, the global consensus variable $\hat{\mathbf{B}}_j[\mathbf{t}]$ is updated by averaging the local SOC trajectories across all subproblems, adjusted by the dual variables. This update brings the consensus closer to the average of what each subproblem believes the SOC should be.

For each battery $j \in \mathcal{B}$ and each time period $t \in \mathcal{T}$:

$$\hat{\mathbf{B}}_j[\mathbf{t}] = \text{clamp} \left(\frac{1}{T} \sum_{t_0=1}^T (\mathbf{B}_j^{\text{to}}[\mathbf{t}] + \mathbf{u}_j^{\text{to}}[\mathbf{t}]), \underline{B}_j, \bar{B}_j \right) \quad (46)$$

where $\underline{B}_j = \text{SOC}_{\min,j} \cdot B_{\text{rated},j}$ and $\bar{B}_j = \text{SOC}_{\max,j} \cdot B_{\text{rated},j}$. The clamping operation ensures that the consensus variable respects the physical SOC bounds.

6.2.4.3 Step 3: Dual Update (Green Variables) Finally, the dual variables $\mathbf{u}_j^{\text{to}}[\mathbf{t}]$ are updated to accumulate the consensus violation (the difference between local and global SOC). These dual variables act as Lagrange multipliers that enforce consensus in the limit as the algorithm converges.

For each battery $j \in \mathcal{B}$, each subproblem $t_0 \in \mathcal{T}$, and each time period $t \in \mathcal{T}$:

$$\mathbf{u}_j^{\text{to}}[\mathbf{t}] := \mathbf{u}_j^{\text{to}}[\mathbf{t}] + (\mathbf{B}_j^{\text{to}}[\mathbf{t}] - \hat{\mathbf{B}}_j[\mathbf{t}]) \quad (47)$$

These three steps are repeated iteratively: solve subproblems for **blue variables**, update consensus **red variables**, and update dual **green variables**, until convergence is achieved.

6.2.5 Convergence Criteria

Primal Residual (Consensus Violation):

The primal residual measures how well the local SOC trajectories $\mathbf{B}_j^{\text{to}}[\mathbf{t}]$ agree with the global consensus $\hat{\mathbf{B}}_j[\mathbf{t}]$ across all batteries and time steps.

$$\|r^k\|_2 = \frac{1}{|\mathcal{B}|} \sqrt{\sum_{j \in \mathcal{B}} \sum_{t=1}^T \left(\frac{1}{T} \sum_{t_0=1}^T \mathbf{B}_j^{t_0}[\mathbf{t}] - \hat{\mathbf{B}}_j[\mathbf{t}] \right)^2} \leq \epsilon_{\text{pri}} \quad (48)$$

Dual Residual (Consensus Change):

The dual residual measures the change in the consensus variable between iterations, indicating convergence stability.

$$\|s^k\|_2 = \frac{\rho}{|\mathcal{B}|} \sqrt{\sum_{j \in \mathcal{B}} \sum_{t=1}^T \left(\hat{\mathbf{B}}_j^k[\mathbf{t}] - \hat{\mathbf{B}}_j^{k-1}[\mathbf{t}] \right)^2} \leq \epsilon_{\text{dual}} \quad (49)$$

6.3 Copper Plate MPOPF with tADMM (Simplified Case)

6.3.1 Problem Overview

To illustrate the tADMM framework more clearly, we first present a simplified copper plate model where network constraints are neglected, and only a single aggregate power balance is enforced at each time step. The Temporal ADMM (tADMM) algorithm decomposes the multi-period optimal power flow problem into T single-step subproblems, each corresponding to one time period. The hope is to enable parallel computation and improved scalability while still retaining solution optimality. Fig. 17 shows the input data for a 24-hour horizon, including the time-varying electricity cost and load demand profiles used in the copper plate MPOPF formulation.

6.3.2 Variable Color Coding

- \mathbf{B}^{t_0} (Blue): Local SOC variables for subproblem t_0
- $\hat{\mathbf{B}}$ (Red): Global consensus SOC trajectory
- \mathbf{u}^{t_0} (Green): Local scaled dual variables for subproblem t_0

6.3.3 tADMM Algorithm Structure

The algorithm alternates between three update steps following the consensus ADMM framework [36, 37]:

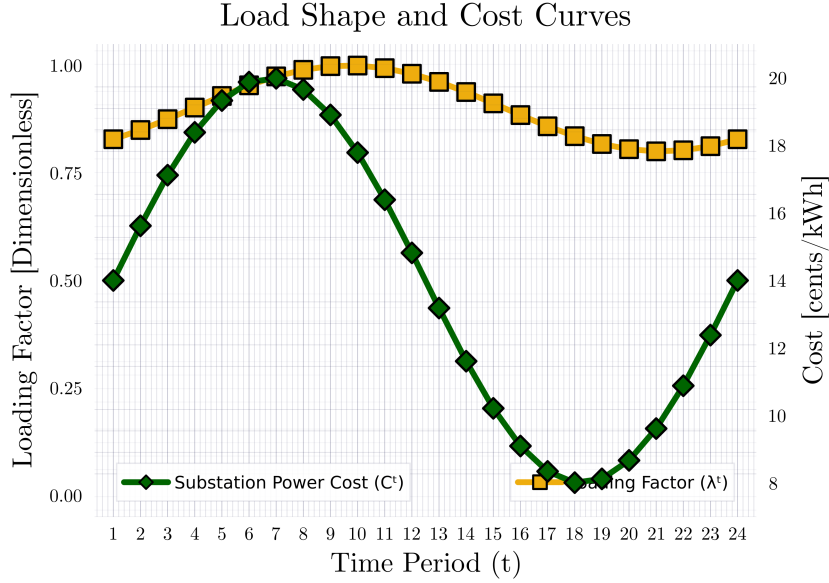


Figure 17: Input curves showing electricity cost and load demand over a 24-hour period.

6.3.3.1 Step 1: Primal Update (Blue Variables) - tADMM Optimization Model

In Update 1 (at iteration k), the latest values of subproblem copies are solved for in parallel using the last known copies of the consensus variable and dual variables – namely $\hat{\mathbf{B}}^{k-1}$ and $\mathbf{u}^{t_0, k-1}$, respectively.

For each subproblem $t_0 \in \{1, 2, \dots, T\}$:

$$\min_{P_{\text{subs}}^{t_0}, P_B^{t_0}, \mathbf{B}^{t_0}} C^{t_0} \cdot P_{\text{subs}}^{t_0} + C_B \cdot (P_B^{t_0})^2 + \frac{\rho}{2} \left\| \mathbf{B}^{t_0} - \hat{\mathbf{B}} + \mathbf{u}^{t_0} \right\|_2^2 \quad (50)$$

Subject to SOC Dynamics for Entire Trajectory:

$$\mathbf{B}^{t_0}[1] = B_0 - P_B^{t_0} \cdot \Delta t \quad (51)$$

$$\mathbf{B}^{t_0}[t] = \mathbf{B}^{t_0}[t-1] - P_B^{t_0} \cdot \Delta t, \quad \forall t \in \{2, \dots, T\} \quad (52)$$

$$P_{\text{subs}}^{t_0} + P_B^{t_0} = P_L[t_0] \quad (53)$$

$$-P_{B,R} \leq P_B^{t_0} \leq P_{B,R} \quad (54)$$

$$\underline{B} \leq \mathbf{B}^{t_0}[t] \leq \bar{B}, \quad \forall t \in \{1, \dots, T\} \quad (55)$$

Key Formulation Notes:

- Each subproblem t_0 optimizes the battery power $P_B^{t_0}$ for *only* time step t_0
- However, the SOC trajectory $\mathbf{B}^{\text{to}}[\mathbf{t}]$ is computed for *all* time steps $t \in \{1, \dots, T\}$
- This ensures that the ADMM penalty term can compare the full trajectory \mathbf{B}^{to} with the consensus $\hat{\mathbf{B}}$
- The power balance constraint is enforced only for the specific time t_0

6.3.3.2 Step 2: Consensus Update (Red Variables) In Update 2 (at iteration k), the latest value of the global consensus variable is computed using the last known copies of the local subproblem SOC trajectories and dual variables – namely $\mathbf{B}_i^{\text{to},k}$ and $\mathbf{u}_i^{\text{to},k-1}$, respectively.

$$\hat{\mathbf{B}}[\mathbf{t}] = \text{clamp} \left(\frac{1}{T} \sum_{t_0=1}^T (\mathbf{B}^{\text{to}}[\mathbf{t}] + \mathbf{u}^{\text{to}}[\mathbf{t}]), \underline{B}, \bar{B} \right) \quad (56)$$

$$\forall t \in \{1, 2, \dots, T-1\} \quad (57)$$

$$\hat{\mathbf{B}}[\mathbf{T}] = B_{T,\text{target}} \quad (\text{if terminal constraint exists}) \quad (58)$$

6.3.3.3 Step 3: Dual Update (Green Variables) In Update 3 (at iteration k), the latest values of local dual variables are computed using the last known copies of the local SOC, global consensus, and previous dual variables – namely $\mathbf{B}_i^{\text{to},k}$, $\hat{\mathbf{B}}^k$, and $\mathbf{u}_i^{\text{to},k-1}$, respectively.

$$\mathbf{u}^{\text{to}}[\mathbf{t}] := \mathbf{u}^{\text{to}}[\mathbf{t}] + (\mathbf{B}^{\text{to}}[\mathbf{t}] - \hat{\mathbf{B}}[\mathbf{t}]) \quad (59)$$

$$\forall t_0 \in \{1, \dots, T\}, \forall t \in \{1, \dots, T\} \quad (60)$$

After every subproblem is solved once to get the latest values of $\mathbf{B}_1, \mathbf{B}_2, \dots, \mathbf{B}_B$, the value of the consensus variable $\hat{\mathbf{B}}$ is updated. Next, the dual variables $\mathbf{u}_1, \mathbf{u}_2, \dots, \mathbf{u}_B$ are updated. This process repeats until convergence.

6.4 Numerical Results

6.4.1 Battery Actions and Convergence Analysis

To validate the tADMM approach, we present numerical results for the copper plate MPOPF problem with a 24-hour planning horizon. The test case includes a single battery energy storage system with time-varying electricity prices and load demands as shown in Fig. 17.

Fig. 18 shows the optimal battery charging and discharging actions obtained from solving the centralized (brute force) MPOPF problem. The battery strategically charges during low-cost periods (typically during nighttime and early morning hours) and discharges during high-cost periods (peak demand hours in the afternoon and evening) to minimize the overall energy cost over the 24-hour horizon. This behavior demonstrates the value of energy arbitrage enabled by battery storage.

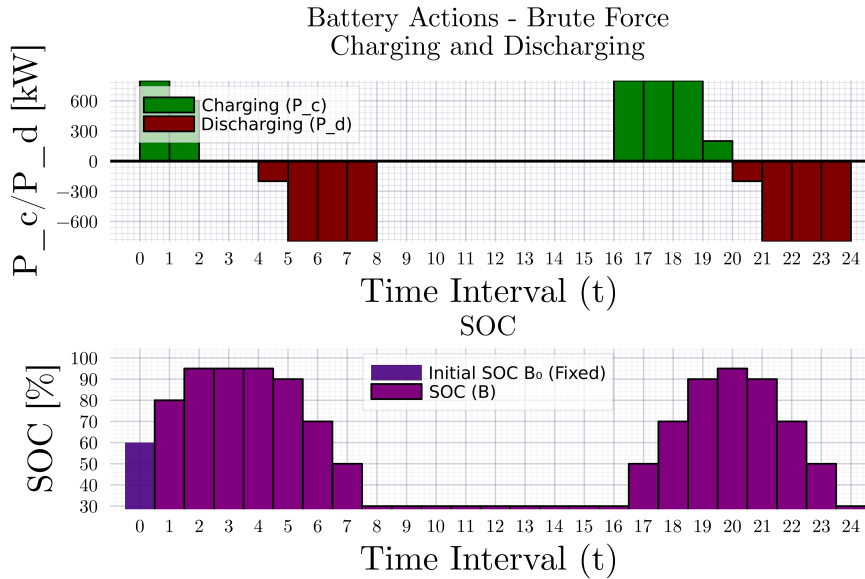


Figure 18: Optimal battery power actions (brute force centralized solution) for copper plate MPOPF over 24-hour horizon. Positive values indicate discharging (supplying power), while negative values indicate charging (consuming power).

Fig. 19 presents the battery actions obtained using the tADMM algorithm, demonstrating that the decomposition approach converges to a solution that closely matches the centralized optimal solution. The close agreement between the two solutions validates the effectiveness of the tADMM decomposition for this problem class. Minor differences, if any, are within the specified convergence tolerances.

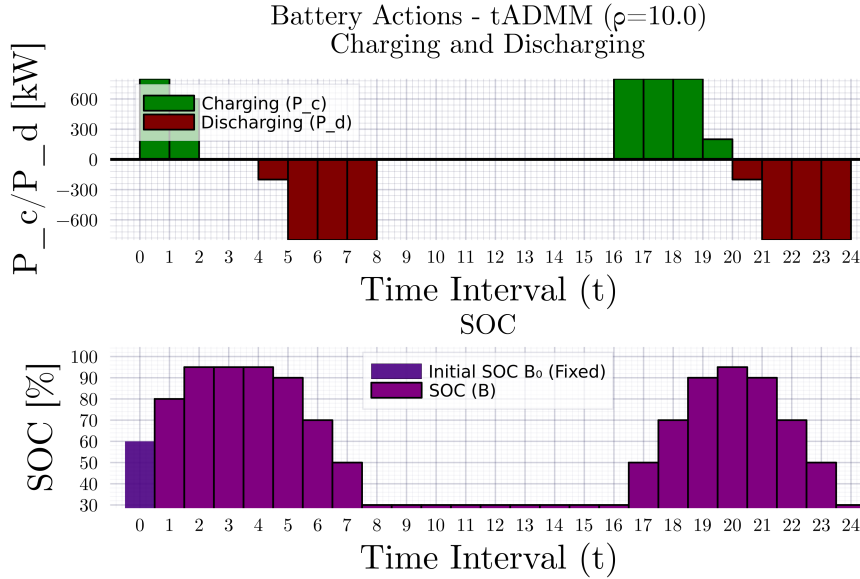


Figure 19: Battery power actions obtained using tADMM for copper plate MPOPF over 24-hour horizon. The solution converges to match the centralized optimal solution.

Fig. 20 illustrates the convergence behavior of the tADMM algorithm, showing how the primal and dual residuals decrease over iterations until they satisfy the specified convergence tolerances ($\epsilon_{\text{pri}} = 10^{-3}$ and $\epsilon_{\text{dual}} = 10^{-3}$). The algorithm typically converges within a few dozen iterations, demonstrating good computational efficiency. The primal residual (consensus violation) decreases as the local SOC trajectories \mathbf{B}^{t_0} converge to the global consensus $\hat{\mathbf{B}}$, while the dual residual tracks the stability of the consensus variable across iterations.

6.5 Convergence Criteria

The algorithm terminates when both residuals fall below specified thresholds:

6.5.1 Convergence Criteria

The algorithm terminates when both residuals fall below specified thresholds:

Primal Residual (Consensus Violation):

The primal residual measures how well the local SOC trajectories \mathbf{B}^{t_0} agree with the global consensus $\hat{\mathbf{B}}$. A small primal residual indicates that all subproblems have converged to a consistent SOC trajectory.

$$\|r^k\|_2 = \left\| \text{vec} \left(\left\{ \mathbf{B}^{t_0} - \hat{\mathbf{B}} \right\}_{t_0=1}^T \right) \right\|_2 \leq \epsilon_{\text{pri}} \quad (61)$$

Dual Residual (Consensus Change):

The dual residual measures how much the consensus variable $\hat{\mathbf{B}}$ is changing between iterations. A small dual residual indicates that the consensus has stabilized.

$$\|s^k\|_2 = \rho \left\| \hat{\mathbf{B}}^k - \hat{\mathbf{B}}^{k-1} \right\|_2 \leq \epsilon_{\text{dual}} \quad (62)$$

6.6 Algorithm Parameters

6.6.1 Objective Function Components

The tADMM objective function for each subproblem t_0 consists of three terms:

$$\text{Energy Cost: } C^{t_0} \cdot P_{\text{subs}}^{t_0} \cdot \Delta t \quad (63)$$

$$\text{Battery Quadratic Cost: } C_B \cdot (P_B^{t_0})^2 \cdot \Delta t \quad (64)$$

$$\text{ADMM Penalty: } \frac{\rho}{2} \left\| B^{t_0} - \hat{B} + u^{t_0} \right\|_2^2 \quad (65)$$

Where:

- C^{t_0} : Energy price at time t_0 [\$/kWh]
- C_B : Battery quadratic cost coefficient [\$/kW²/h] (typically $10^{-6} \times \min(C^t)$)
- ρ : ADMM penalty parameter

The battery quadratic cost term $C_B \cdot (P_B^{t_0})^2$ serves as a regularization to:

1. Prevent excessive battery cycling
2. Encourage smoother power trajectories
3. Improve numerical conditioning of the optimization problem

6.6.2 Algorithmic Parameters

- **Penalty Parameter:** ρ (typically 0.1 to 10.0)
- **Primal Tolerance:** $\epsilon_{\text{pri}} = 10^{-3}$
- **Dual Tolerance:** $\epsilon_{\text{dual}} = 10^{-3}$
- **Maximum Iterations:** 1000

6.7 Appendix: Full Variable and Parameter Definitions

6.7.1 System Bases

$$\text{kV}_B = \frac{4.16}{\sqrt{3}} \text{ kV} \text{ (phase-to-neutral)} \quad (66)$$

$$\text{kVA}_B = 1000 \text{ kVA} \quad (67)$$

$$P_{\text{BASE}} = 1000 \text{ kW} \quad (68)$$

$$E_{\text{BASE}} = 1000 \text{ kWh per hour} \quad (69)$$

6.7.2 SOC Bound Definitions

$$\underline{B} = \text{SOC}_{\min} \cdot E_{\text{Rated}} \quad (70)$$

$$\overline{B} = \text{SOC}_{\max} \cdot E_{\text{Rated}} \quad (71)$$

6.7.3 Physical Interpretation

- $P_B[t] > 0$: Battery discharging (providing power to the system)
- $P_B[t] < 0$: Battery charging (consuming power from the system)
- $B[t]$: Battery state of charge at the end of period t
- $\underline{B} = \text{SOC}_{\min} \cdot E_{\text{Rated}}$: Lower SOC bound
- $\overline{B} = \text{SOC}_{\max} \cdot E_{\text{Rated}}$: Upper SOC bound

6.8 Summary and Discussion

The temporal ADMM (tADMM) approach provides an effective decomposition framework for solving multi-period optimal power flow problems with energy storage. The key advantages of this approach include:

- **Parallelization:** Each time-step subproblem can be solved independently and in parallel, enabling computational speedup on multi-core processors or distributed computing platforms
- **Modularity:** The decomposition structure is flexible and can accommodate different network models (LinDistFlow, AC power flow, copper plate) without changing the temporal decomposition framework
- **Scalability:** The computational complexity scales more favorably with the number of time periods compared to solving the full centralized problem
- **Convergence guarantees:** For convex formulations, ADMM provides theoretical convergence guarantees to the global optimum [36, 37]

The numerical results demonstrate that tADMM successfully decomposes the temporal coupling through battery SOC while maintaining solution optimality. The algorithm converges within a reasonable number of iterations, and the final solution matches the centralized optimal solution within the specified tolerances. This validates the effectiveness of the consensus-based decomposition for handling temporal coupling in MPOPF problems.

6.8.1 Implementation Status

The tADMM framework has been developed and tested with varying levels of network model complexity:

- **Copper Plate Model (Completed):** The tADMM algorithm has been successfully implemented and tested for the simplified copper plate MPOPF problem. The numerical results presented in Figs. 18, 19, and 20 demonstrate successful convergence to the optimal solution, validating the temporal decomposition approach.
- **LinDistFlow Model (In Progress):** The tADMM formulation with the linearized DistFlow model [38] is currently being implemented. This will incorporate spatial

network constraints including voltage limits, line flow limits, and reactive power constraints while maintaining the temporal decomposition structure.

- **Nonlinear Branch Flow Model (Planned):** Future work will extend the tADMM framework to the SOCP-relaxed nonlinear branch flow model (BFM) [4]. This represents the true nonlinear MPOPF problem with exact AC power flow physics. The BFM formulation will provide a more accurate representation of distribution network behavior while benefiting from the computational advantages of temporal decomposition. This will showcase the full potential of tADMM for solving realistic large-scale MPOPF problems with complex network constraints.

Future extensions of this work will focus on:

- Completing the LinDistFlow implementation and validating performance on realistic distribution networks
- Implementing the SOCP-relaxed BFM formulation with tADMM decomposition
- Applying tADMM to larger distribution networks with multiple batteries and renewable energy sources
- Investigating adaptive penalty parameter selection strategies to improve convergence speed
- Integrating spatial decomposition techniques with temporal decomposition for enhanced scalability

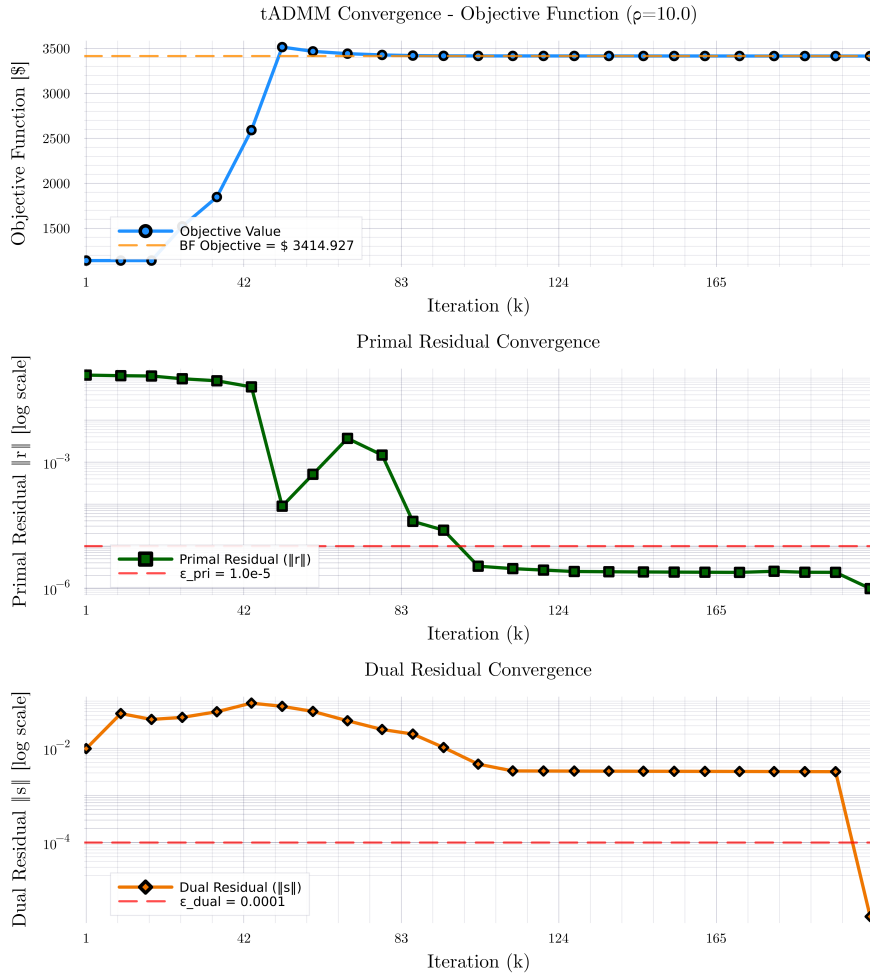


Figure 20: Convergence curves showing primal and dual residuals for tADMM algorithm. Both residuals decrease monotonically and satisfy the convergence criteria.

7 Future Works

The proposed future work aims to extend the temporal decomposition framework developed in this research to larger and more complex power distribution systems. The timeline for completion spans three semesters from Fall 2025 through Summer 2026, culminating in dissertation preparation and defense. The work is organized into three main tasks that progressively scale the methodology and conclude the doctoral research.

7.1 Task 1: Temporal Decomposition for Medium Sized Balanced Three-Phase Systems

The first task focuses on developing and validating the temporal decomposition approach for medium-scale distribution systems assuming balanced three-phase conditions. So far the mathematical framework for temporal decomposition using tADMM has been established, extending the concepts developed in earlier work to handle time-coupled constraints and multi-period optimization problems. The formulation phase will establish the theoretical foundations and decomposition strategy.

Following the formulation, implementation and testing will be conducted on the IEEE 123-bus single-phase test system. This medium-scale system provides sufficient complexity to validate the decomposition approach while remaining computationally tractable for initial testing. The implementation will focus on developing efficient algorithms and testing convergence properties. This task is scheduled for completion during Fall 2025.

7.2 Task 2: Temporal Decomposition for Large Sized Unbalanced Three-Phase Systems

The second task scales the temporal decomposition methodology to large-scale three-phase distribution systems. Building on the insights from Task 1, this phase will formulate the decomposition approach specifically for three-phase unbalanced systems, accounting for the additional complexity of phase coupling and imbalance.

The implementation and testing will be performed on the IEEE 9500-bus three-phase test system, which represents a realistic large-scale distribution network. This task will demonstrate the scalability of the temporal decomposition approach and validate its effectiveness on industry-relevant system sizes. The work is planned for completion during Spring 2026.

7.3 Task 3: Concluding Research and Dissertation

The final task encompasses completion of remaining research activities and dissertation preparation. This includes finishing the investigation of differential dynamic programming (DDP) methods, conducting a comprehensive literature review on novel temporal decomposition methods in power systems, and completing any remaining implementations or case studies.

The dissertation preparation and defense phase will synthesize all research contributions, document the methodologies and results, and prepare for the final defense. This task spans from late Spring 2026 through Summer 2026, concluding the doctoral research program.

7.4 Timeline

The timeline for the research efforts as detailed in Section 7 is shown in Fig. 21.

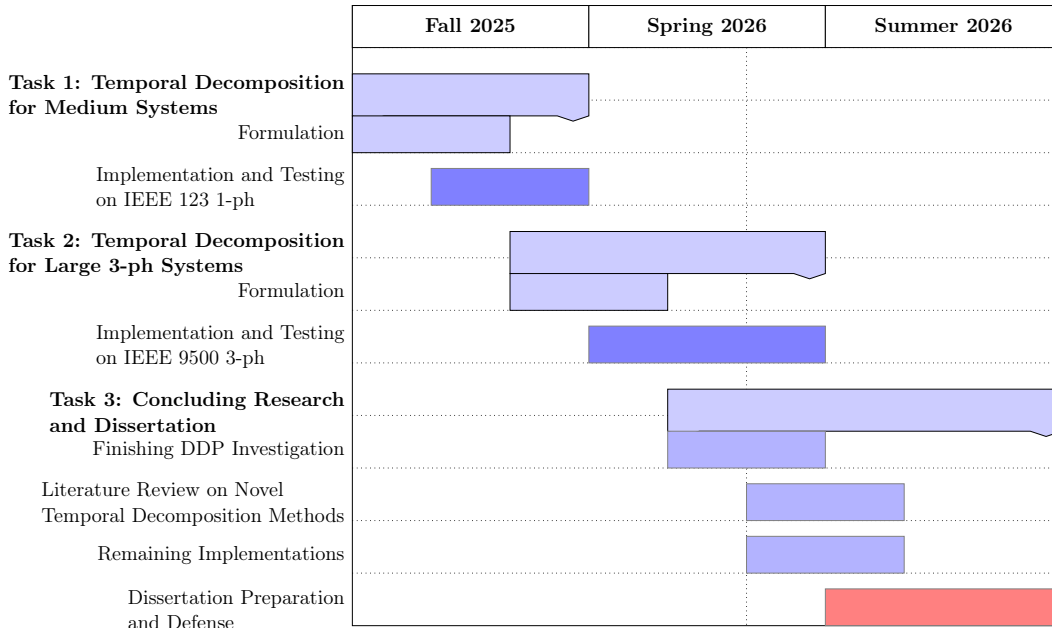


Figure 21: Gantt chart showing execution plan for future works.

8 Biography

Aryan Ritwajeet Jha received the B.E. degree in Electrical and Electronics Engineering from the Birla Institute of Technology and Science (BITS) Pilani, India, in 2020. He is currently pursuing his Ph.D. in Electrical Engineering at Washington State University, Pullman, WA, USA. His research interests include power distribution system optimization, scalable decomposition algorithms for large-scale non-linear optimization and optimization solvers.

8.1 Publications

1. **Jha, A. R.**, Paul, S., & Dubey, A. . Spatially Distributed Multi-Period Optimal Power Flow with Battery Energy Storage Systems. 2024 56th North American Power Symposium (NAPS). IEEE. doi: 10.1109/NAPS61145.2024.10741846 [1]
2. **Jha, A. R.**, Paul, S., & Dubey, A. . Analyzing the Performance of Linear and Nonlinear Multi -Period Optimal Power Flow Models for Active Distribution Networks. 2025 IEEE North-East India International Energy Conversion Conference and Exhibition (NE-IECCE). IEEE. doi: 10.1109/NE-IECCE64154.2025.11183479 [8]

8.2 Program of Study Course Work

Course Number and Name	Semester	Instructor	Grade
E_E 507 Random Processes in Engineering	Fall 2022	Prof. Sandip Roy	A
E_E 521 Analysis of Power Systems	Fall 2022	Prof. Noel Schulz	A
E_E 523 Power Systems Stability	Spring 2023	Prof. Mani V. Venkatasubramanian	A
MATH 564 Convex and Nonlinear Optimization	Fall 2023	Prof. Tom Asaki	A
MATH 565 Nonsmooth Analysis and Optimization	Spring 2024	Prof. Tom Asaki	A-
CPT_S 530 Numerical Analysis ¹	Fall 2025	Prof. Alexander Panchenko	
E_E 582 Electrical Systems Modelling and Simulation ¹	Fall 2025	Prof. Seyedmilad Ebrahimi	
E_E 595 Directed Studies in Electrical Engineering ¹	Fall 2025	Prof. Rahul K. Gupta	

¹

¹currently taking this semester

Appendix

In Section .1 from Equations (72) to (84), the full optimization formulation for the Multi-Period Optimal Power Flow (MPOPF) problem using the LinDistFlow model is presented.

.1 Full MPOPF Formulation with LinDistFlow

Sets:

- \mathbb{N} : Set of all buses, with substation bus $j_1 \in \mathbb{N}$
- $\mathbb{N} \setminus \{j_1\}$: Set of non-substation buses
- \mathbb{L} : Set of all branches (directed edges)
- \mathbb{L}_1 : Set of branches directly connected to substation bus j_1
- $\mathbb{L} \setminus \mathbb{L}_1$: Set of branches not connected to substation
- \mathbb{B} : Set of buses with battery storage
- \mathbb{D} : Set of buses with distributed energy resources (DERs)
- \mathbb{T} : Set of time periods $\{1, 2, \dots, T\}$

Objective Function:

$$\min \sum_{t \in \mathbb{T}} C^t P_{\text{Subs}}^t \Delta t + \sum_{t \in \mathbb{T}} \sum_{j \in \mathbb{B}} C_B (P_{B_j}^t)^2 \Delta t \quad (72)$$

Subject to:

Power Balance at Substation Bus ($j = j_1$):

$$P_{\text{Subs}}^t - \sum_{(j_1, k) \in \mathbb{L}_1} P_{j_1 k}^t = 0, \quad \forall t \in \mathbb{T} \quad (73)$$

$$Q_{\text{Subs}}^t - \sum_{(j_1, k) \in \mathbb{L}_1} Q_{j_1 k}^t = 0, \quad \forall t \in \mathbb{T} \quad (74)$$

Power Balance at Non-Substation Buses ($j \in \mathbb{N} \setminus \{j_1\}$):

$$\sum_{(j, k) \in \mathbb{L}} P_{jk}^t - \sum_{(i, j) \in \mathbb{L}} P_{ij}^t = P_{B_j}^t + p_{D_j}^t - p_{L_j}^t, \quad \forall j \in \mathbb{N}, \forall t \in \mathbb{T} \quad (75)$$

$$\sum_{(j, k) \in \mathbb{L}} Q_{jk}^t - \sum_{(i, j) \in \mathbb{L}} Q_{ij}^t = q_{D_j}^t - q_{L_j}^t, \quad \forall j \in \mathbb{N}, \forall t \in \mathbb{T} \quad (76)$$

Voltage Drop (LinDistFlow KVL):

$$v_j^t = v_i^t - 2(r_{ij}P_{ij}^t + x_{ij}Q_{ij}^t), \quad \forall(i, j) \in \mathbb{L}, \forall t \in \mathbb{T} \quad (77)$$

Substation Voltage:

$$v_{j_1}^t = v_{\text{nom}}^2, \quad \forall t \in \mathbb{T} \quad (78)$$

Voltage Limits:

$$(v_{\min})^2 \leq v_j^t \leq (v_{\max})^2, \quad \forall j \in \mathbb{N}, \forall t \in \mathbb{T} \quad (79)$$

Battery State of Charge:

$$B_j^t = B_j^{t-1} - P_{B_j}^t \Delta t, \quad \forall j \in \mathbb{B}, \forall t \in \mathbb{T} \setminus \{1\} \quad (80)$$

$$B_j^1 = B_{j,0}, \quad \forall j \in \mathbb{B} \quad (81)$$

Battery Constraints:

$$\text{SOC}_{\min} B_{R_j} \leq B_j^t \leq \text{SOC}_{\max} B_{R_j}, \quad \forall j \in \mathbb{B}, \forall t \in \mathbb{T} \quad (82)$$

$$-P_{B_{R_j}} \leq P_{B_j}^t \leq P_{B_{R_j}}, \quad \forall j \in \mathbb{B}, \forall t \in \mathbb{T} \quad (83)$$

PV Reactive Power Limits:

$$-\sqrt{S_{D_{R_j}}^2 - (p_{D_j}^t)^2} \leq q_{D_j}^t \leq \sqrt{S_{D_{R_j}}^2 - (p_{D_j}^t)^2}, \quad \forall j \in \mathbb{D}, \forall t \in \mathbb{T} \quad (84)$$

Variables:

- $P_{\text{Subs}}^t, Q_{\text{Subs}}^t$: Substation real and reactive power at time t
- P_{ij}^t, Q_{ij}^t : Sending-end real and reactive power flow on branch (i, j) at time t
- v_j^t : Squared voltage magnitude at bus j at time t
- $P_{B_j}^t$: Battery power at bus j at time t (positive = discharging)
- B_j^t : Battery state of charge at bus j at time t
- $q_{D_j}^t$: PV reactive power injection at bus j at time t

Parameters:

- C^t : Energy cost at time t (\$/kWh)
- C_B : Battery degradation cost coefficient
- Δt : Time step duration

- r_{ij}, x_{ij} : Branch resistance and reactance
- $p_{L_j}^t, q_{L_j}^t$: Load real and reactive power at bus j at time t
- $p_{D_j}^t$: PV real power generation at bus j at time t
- $B_{R_j}, P_{B_{R_j}}$: Battery energy and power capacity at bus j
- $S_{D_{R_j}}$: PV apparent power capacity at bus j

References

- [1] A. R. Jha, S. Paul, and A. Dubey, “Analyzing the Performance of Linear and Nonlinear Multi - Period Optimal Power Flow Models for Active Distribution Networks,” *Published in: 2025 IEEE North-East India International Energy Conversion Conference and Exhibition (NE-IECCE)*, pp. 04–06.
- [2] N. Nazir, P. Racherla, and M. Almassalkhi, “Optimal multi-period dispatch of distributed energy resources in unbalanced distribution feeders,” *arXiv*, Jun. 2019.
- [3] A. Agarwal and L. Pileggi, “Large Scale Multi-Period Optimal Power Flow With Energy Storage Systems Using Differential Dynamic Programming,” *IEEE Trans. Power Syst.*, vol. 37, no. 3, pp. 1750–1759, Sep. 2021.
- [4] M. Farivar and S. H. Low, “Branch Flow Model: Relaxations and Convexification—Part I,” *IEEE Trans. Power Syst.*, vol. 28, no. 3, pp. 2554–2564, Apr. 2013.
- [5] A. Gabash and P. Li, “Active-reactive optimal power flow in distribution networks with embedded generation and battery storage,” *IEEE Trans. Power Syst.*, vol. 27, no. 4, pp. 2026–2035, Nov. 2012.
- [6] N. Nazir and M. Almassalkhi, “Receding-Horizon Optimization of Unbalanced Distribution Systems with Time-Scale Separation for Discrete and Continuous Control Devices,” *2018 Power Systems Computation Conference (PSCC)*, pp. 1–7, Jun. 2018.
- [7] L. Gan, U. Topcu, and S. H. Low, “Convex Relaxation of Optimal Power Flow Part I: Formulations and Equivalence,” in *IEEE Transactions on Power Systems*, 2015, vol. 30, no. 1, pp. 290–301.
- [8] A. R. Jha, S. Paul, and A. Dubey, “Spatially Distributed Multi-Period Optimal Power Flow with Battery Energy Storage Systems,” *Published in: 2024 56th North American Power Symposium (NAPS)*, pp. 13–15.
- [9] G. Valverde, E. M. G. de Oliveira, A. M. V. de Lara, J. R. S. Peres, and N. Favilla, “Multiperiod optimum power flow for active distribution networks incorporating distributed generation and energy storage systems,” *IEEE Transactions on Industry Applications*, 2021. [Online]. Available: <https://ieeexplore.ieee.org/document/9502092/>
- [10] A. G. B. et al., “Large scale multi-period optimal power flow with energy storage,” *IEEE Transactions on Power Systems*, 2021. [Online]. Available: <https://ieeexplore.ieee.org/document/9549701/>
- [11] ———, “Large scale multi-period optimal power flow with energy storage,” *IEEE Transactions on Power Systems*, 2021. [Online]. Available: <https://ieeexplore.ieee.org/document/9549701/>

- [12] C. Wu, W. Gu, S. Zhou, and X. Chen, “Coordinated optimal power flow for integrated active distribution network and virtual power plants using decentralized algorithm,” *IEEE Trans. Power Syst.*, vol. 36, no. 4, pp. 3541–3551, Jul. 2021.
- [13] M. Farivar and S. H. Low, “Branch flow model: Relaxations and convexification—part i,” *IEEE Trans. Power Syst.*, vol. 28, no. 3, pp. 2554–2564, 2013.
- [14] N. Nazir and M. Almassalkhi, “Guaranteeing a Physically Realizable Battery Dispatch Without Charge-Discharge Complementarity Constraints,” *IEEE Trans. Smart Grid*, vol. 14, no. 3, pp. 2473–2476, Sep. 2021.
- [15] H. Ahmadi and J. R. Martí, “Linear Current Flow Equations With Application to Distribution Systems Reconfiguration,” *IEEE Trans. Power Syst.*, vol. 30, no. 4, pp. 2073–2080, Oct. 2014.
- [16] A. Wächter and L. T. Biegler, “On the implementation of an interior-point filter line-search algorithm for large-scale nonlinear programming,” *Math. Program.*, vol. 106, no. 1, pp. 25–57, Mar. 2006.
- [17] M. Lubin, O. Dowson, J. Dias Garcia, J. Huchette, B. Legat, and J. P. Vielma, “JuMP 1.0: Recent improvements to a modeling language for mathematical optimization,” *Mathematical Programming Computation*, vol. 15, p. 581–589, 2023.
- [18] “OpenDSSDirect.jl,” Mar. 2025, [Online; accessed 9. Mar. 2025]. [Online]. Available: <https://github.com/dss-extensions/OpenDSSDirect.jl>
- [19] “MultiPeriod-DistOPF-Benchmark,” Jul. 2024, [Online; accessed 15. Jul. 2024]. [Online]. Available: <https://github.com/Realife-Brahmin/MultiPeriod-DistOPF-Benchmark>
- [20] T. Gangwar, N. P. Padhy, and P. Jena, “Storage allocation in active distribution networks considering life cycle and uncertainty,” *IEEE Trans. Ind. Inform.*, vol. 19, no. 1, pp. 339–350, Jan. 2023.
- [21] S. Paul and N. P. Padhy, “Real-time advanced energy-efficient management of an active radial distribution network,” *IEEE Syst. J.*, vol. 16, no. 3, pp. 3602–3612, Sept. 2022.
- [22] W. Wei, J. Wang, and L. Wu, “Distribution optimal power flow with real-time price elasticity,” *IEEE Trans. Power Syst.*, vol. 33, no. 1, pp. 1097–1098, Jan. 2018.
- [23] M. M.-U.-T. Chowdhury, B. D. Biswas, and S. Kamalasadan, “Second-order cone programming (socp) model for three phase optimal power flow (opf) in active distribution networks,” *IEEE Trans. Smart Grid*, vol. 14, no. 5, pp. 3732–3743, 2023.
- [24] Z. Guo, W. Wei, L. Chen, Z. Dong, and S. Mei, “Parametric distribution optimal power flow with variable renewable generation,” *IEEE Trans. Power Syst.*, vol. 37, no. 3, pp. 1831–1841, May 2022.

- [25] H. Yuan, F. Li, Y. Wei, and J. Zhu, “Novel linearized power flow and linearized opf models for active distribution networks with application in distribution lmp,” *IEEE Trans. Smart Grid*, vol. 9, no. 1, pp. 438–448, Jan. 2018.
- [26] A. R. Di Fazio, C. Risi, M. Russo, and M. De Santis, “Decentralized voltage optimization based on the auxiliary problem principle in distribution networks with ders,” *Appl. Sci.*, vol. 11, no. 4509, pp. 1–24, 2021.
- [27] W. Zheng, W. Wu, B. Zhang, H. Sun, and Y. Liu, “A fully distributed reactive power optimization and control method for active distribution networks,” *IEEE Trans. Smart Grid*, vol. 7, no. 2, pp. 1021–1033, Mar. 2016.
- [28] P. Wang, Q. Wu, S. Huang, C. Li, and B. Zhou, “Admm-based distributed active and reactive power control for regional ac power grid with wind farms,” *J. Modern Power Syst. Clean Energy*, vol. 10, no. 3, pp. 588–596, May 2022.
- [29] B. D. Biswas, M. S. Hasan, and S. Kamalasadan, “Decentralized distributed convex optimal power flow model for power distribution system based on alternating direction method of multipliers,” *IEEE Trans. Ind. Appl.*, vol. 59, no. 1, pp. 627–640, Jan.-Feb. 2023.
- [30] S. Paul, B. Ganguly, and S. Chatterjee, “Nesterov-type accelerated admm (n-admm) with adaptive penalty for three-phase distributed opf under non-ideal data transfer scenarios,” in *2023 IEEE 3rd International Conference on Smart Technologies for Power, Energy and Control (STPEC)*, 2023, pp. 1–6.
- [31] R. Sadnan and A. Dubey, “Distributed optimization using reduced network equivalents for radial power distribution systems,” *IEEE Trans. Power Syst.*, vol. 36, no. 4, pp. 3645–3656, Jul. 2021.
- [32] M. Alizadeh and V. Capitanescu, “Stochastic security-constrained multi-period optimal power flow,” *Electric Power Systems Research*, vol. 189, p. 106660, 2020.
- [33] M. Usman and V. Capitanescu, “Multi-period ac optimal power flow: Formulations and solution methods,” *IEEE Transactions on Power Systems*, vol. 32, no. 4, pp. 3268–3277, 2017.
- [34] A. R. Aghdam and M. Shahidehpour, “Optimal battery scheduling for renewable integration using model predictive control,” *IEEE Transactions on Sustainable Energy*, vol. 10, no. 1, pp. 211–220, 2019.
- [35] X. Zhang, X. Yuan, and J. Zhang, “A robust bi-level multi-period optimal dispatch method for distribution networks with ders,” *IEEE Transactions on Power Systems*, vol. 36, no. 3, pp. 2306–2316, 2021.
- [36] “ADMM,” Oct. 2025, [Online; accessed 28. Oct. 2025]. [Online]. Available: <https://stanford.edu/~boyd/admm.html>

- [37] “Index of `/~ryantibs/convexopt-F16/lectures`,” Oct. 2025, [Online; accessed 28. Oct. 2025]. [Online]. Available: <https://www.stat.cmu.edu/~ryantibs/convexopt-F16/lectures>
- [38] M. E. Baran and F. F. Wu, “Optimal capacitor placement on radial distribution systems,” *IEEE Transactions on Power Delivery*, vol. 4, no. 1, pp. 725–734, 1989.